Fluidic Delivery Line for Naphtha Detection

by

Gunjan Singh

A thesis submitted in partial fulfillment of the requirements for the degree of

Master of Science
in
Chemical Engineering

Department of Chemical and Materials Engineering

University of Alberta

Abstract

Naphtha that consists of low molecular weight aliphatic and aromatics and other low molecular weight iso-paraffins and naphthenes is used as a diluent in processing of bitumen from oil sands. During oil sands processing, almost all of the naphtha is recovered. However, a small fraction, viz. <1%, is lost to tailings waste and is incorporated into mature fine tailings. Presently, a sample of mature fine tailings is collected and transported to laboratory every 6 hours to monitor its naphtha content using Gas Chromatography Mass Spectrometry. This method of detecting naphtha is time consuming, expensive and requires trained personnel. Above all, it does not allow for real-time detection. To meet the demand of real-time naphtha detection in mature fine tailings, an approach for design and development of fluidic delivery line as processing unit for naphtha sensor has been made.

In this study, a compact and portable fluidic delivery system is devised that combines the filtration unit, the pumping system and the heating system in a static cell for Naphtha detection. The filtration unit makes the processed water devoid of impurities like clay particles and sand. A droplet system is used to pour the filtered sample on a copper sheet that serves as hot plate for the heating system. The vaporized sample is pulled out and delivered to the micro cantilever that detects naphtha. A miniaturized design using a microfluidic filtration unit and a liquid-vapor separation chip is also proposed. The proposed fluidic delivery line can be used for any available liquid.

Acknowledgment

I would like to express my sincere gratitude to my supervisor Dr. Neda Nazemifard for her guidance and immense support throughout the course of my research. I would be forever thankful for her wonderful advices and for making me believe in myself through highs and lows.

I would like to take this opportunity to extend special thanks to Dr. Thomas Thundat for his invaluable help and endless support. I would also like to thank Mr. Walter Boddez, David Parlin and Jeremy for their time and approachable nature to help wherever my work demanded.

Not to forget the help received from my lab mates and colleagues in discussing project and receive their undeniable support. I would like to thank Muhammad, Kevin, Insoek and Arindam in this regard. I would like to extend my thanks to the wonderful staff of Department of Chemical and Material Engineering and Institute for Oil Sands Innovation at the University of Alberta.

Last but not the least, I gratefully acknowledge the financial support received from NSERC CRD and Institute for Oil Sands Innovation.

Table of Contents

List of Figures

List of Tables

Chapter 1 Introduction

Various types of heavy oil deposits are found in the world, major reserves occurring in Alaska (in the United States), Alberta (in Canada), and Orinoco belt (in Venezuela). Unlike oil deposits found in Orinoco belt and Alaska, Alberta's deposits are made of oil sands, which are a naturally occurring mixture of crude bitumen, rock matrix, water and clays. It is also known as tar sand or bituminous sands. Bitumen is highly viscous hydrocarbon mixture that appears like cold molasses at room temperature. Collectively, Alberta has the highest hydrocarbon deposits and ranks second in the world in terms of oil reserves, after Saudi Arabia. (Masliyah, Xu et al. 2011)

1.1 Overview of Oil Sands

It is believed that a member of Northwest West Company, Peter Pond, first examined oil sands in 1778. However, it was not until late 1920s that research began in extracting bitumen from the oil sands. (Masliyah, Xu et al. 2011) Dr. Karl Clark identified a process to recover bitumen from oil sands in 1927. He used water to separate bitumen, which later was known as Clark Hot Water Extraction process. (Clark, Blair et al. 1927) CHWE process was initially used in construction industry. Recovery of bitumen for production of fuel oil began in the 1950s when new technologies were adopted. (Blair 1951) In the late 1960s, better operations were developed that comprised of three parts: open-pit mining, hot water extraction unit and an upgrading system to convert heavy bitumen into light synthetic crude. Producing synthetic crude from mineable oil sands was difficult and expensive in the beginning. However, introduction of new in situ production technology, construction materials and their handling led to better means of extracting bitumen and upgrading them at a reduced cost. (Masliyah, Xu et al. 2011)

The quality of oil sand deposits is determined by weight percentage of the bitumen content and the thickness of bitumen zone. An ore with a bitumen content ranging from 7-16 % is used for commercial purposes, with 7% being the minimum grade cut-off. Oil

sands ore typically contains 9%-13% bitumen, 3%-7% water, and 80%-85% mineral solids. Fine particles, predominantly clay, constitute 15%-30% of the solid content. One of the major challenges faced until date is to remove the fine clays during bitumen extraction, other than removing bitumen from coarser sand grains. (Masliyah, Gray et al. 2006) Takamura suggested a model for microscopic structure of oil sand having a thin water layer on a sand grain. (Takamura 1982) This is shown in Figure 1. (Masliyah, Xu et al. 2011)

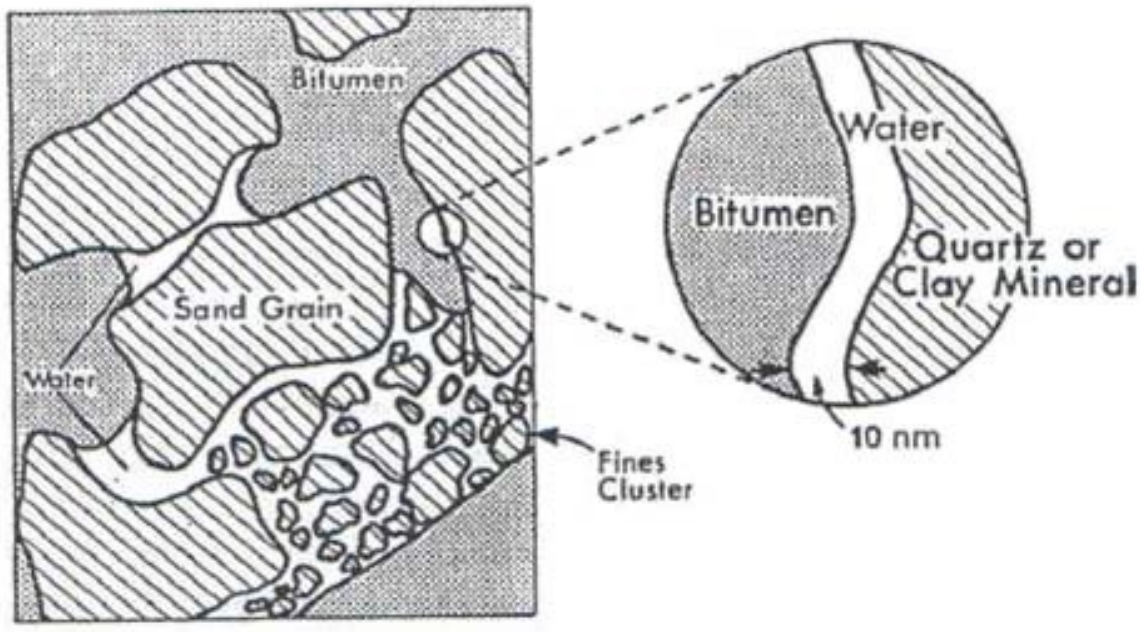

Figure 1 Model showing microscopic structure of Athabasca oil sands as proposed by Takamura (Masliyah, Xu et al. 2011)

Canada's crude bitumen reserves are present in three oil sands area-namely, Athabasca Wabiskaw McMurray, Cold Lake Clearwater and Peace River Bluesky-Gething. Oil sands are assumed to have been formed by biogenic process wherein alterations with biomass was caused under varied conditions, mentioned differently by different theories. (Masliyah, Xu et al. 2011)

Currently, two methods are employed to recover bitumen from the Athabasca oil sands-namely, Open pit mining and In-situ. Overburden and muskeg are scraped off to

exposed oil sands surfaces in the former. A number of means are used for scrapping the layer above oil sand belt, truck and shovel method being among the widely used methods. For a deep overburden (thickness > 75m), in-situ methods are used. These methods include Steam-assisted gravity drainage, Toe to heal air injection, Cyclic steam stimulation and Vapor extraction. Presently, Steam-assisted gravity drainage and cyclic steam simulation are widely used in industrial practice. (Masliyah, Xu et al. 2011)

According to latest updates on oil sands by Energy Resources Conservation Board of Alberta, 2012 (ERCB 2012) bitumen production is likely to double by 2017 to 3.23 million from 1.32 million in 2007. Synthetic crude oil production has increased by 4% since 2007. Among the three major oil sands deposits areas of Alberta, Athabasca with both mining and in-situ mining projects produces most bitumen. Two major by-products obtained from bitumen upgrading processes are sulfur and petroleum coke.

1.2 Naphtha in bitumen extraction process and tailings

Naphtha is mixture of low molecular weight aliphatic and aromatics, having compounds with 7-14 carbon atoms, and other low molecular weight iso-paraffins and naphthenes. It is used as a diluent in processing bitumen from oil sands. (Siddique, Fedorak et al. 2007) US patent 20130240412A1 directs the use of Naphtha for cleaning bitumen froth by mixing naphtha with the bitumen froth to a naphtha-to-bitumen ratio (by weight) ranging from 4.0 to 10.0. Furthermore, an adequate amount of Naphtha is also used with diluted bitumen to separate marketable raw bitumen from sands and water. Naphtha facilitates reduction of bitumen froth viscosity. There are several other methods used to reduce viscosity of bitumen, viz., heating, upgrading, core annular flow and water in oil emulsion formation (Homayuni, Hamidi et al. 2012)

Liberation and aeration of bitumen are largely affected by bitumen viscosity. There are two ways by which viscosity of bitumen can be reduced: addition of a diluent or increasing the temperature. It has been researched that bitumen enclosing the sand grains may remain intact in water if viscous forces exceed the capillary forces. This could result in a poor bitumen separation from the sand grains, if any. (Najafi, Drelich et al. 2007) It

is important to note that at higher temperature, effectiveness of solvent in bitumen processing decreases. Figure 2 shows Athabasca bitumen viscosity reduction by addition of naphtha (w%) (Masliyah, Xu et al. 2011)

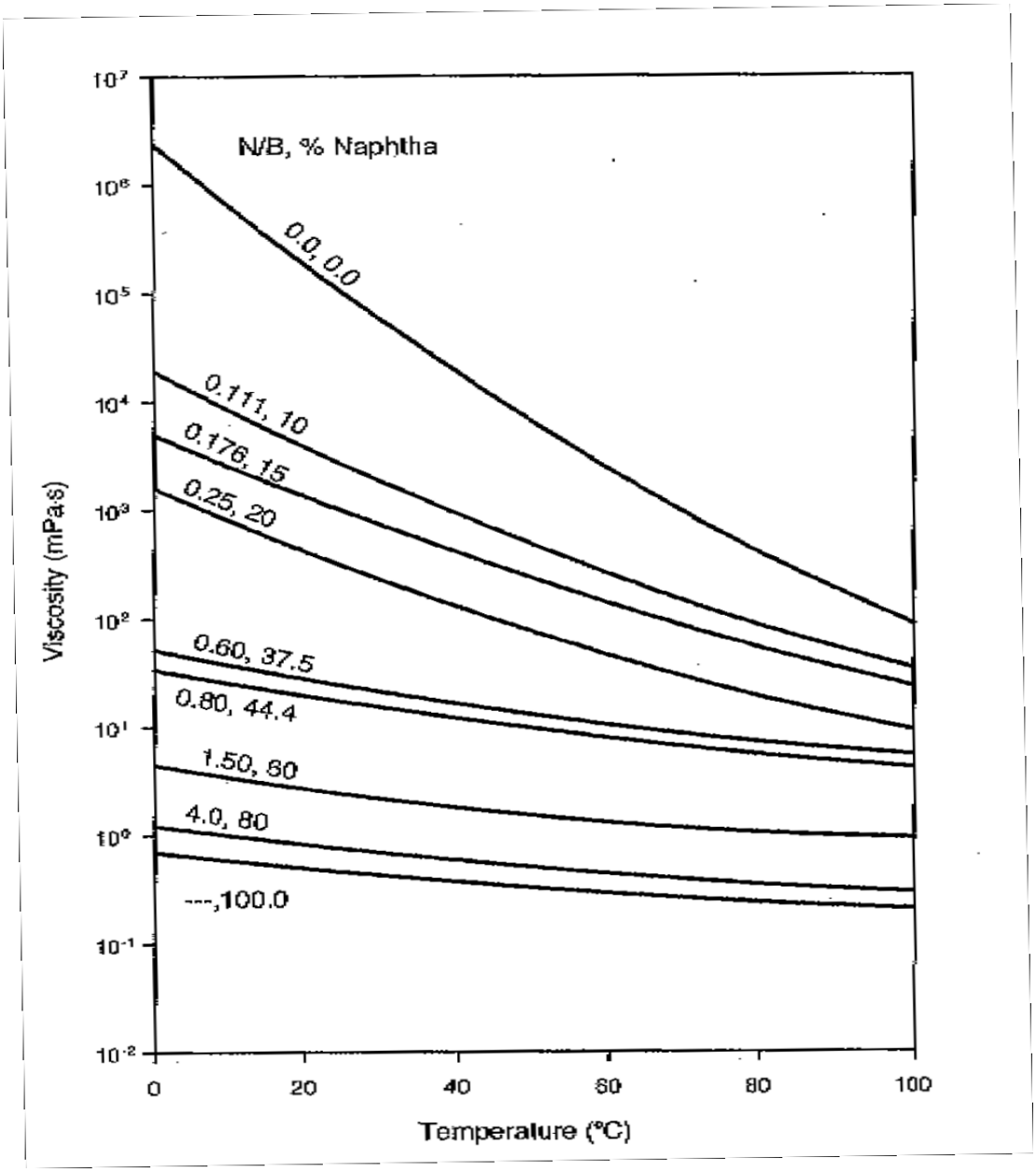

Figure 2 Athabasca bitumen viscosity reduction by addition of naphtha (wt%) (Masliyah, Xu et al. 2011)

Naphtha is recovered from the bitumen froth treatment unit by feeding the mixture to diluent recovery unit. Bitumen produced in Alberta is piped to US PADD2 refinery as dilbit (naphtha diluent and bitumen). The recovered naphtha is brought back to Alberta. Figure 3 shows a photomicrograph of naphtha-diluted bitumen after centrifugation. (Masliyah, Xu et al. 2011)

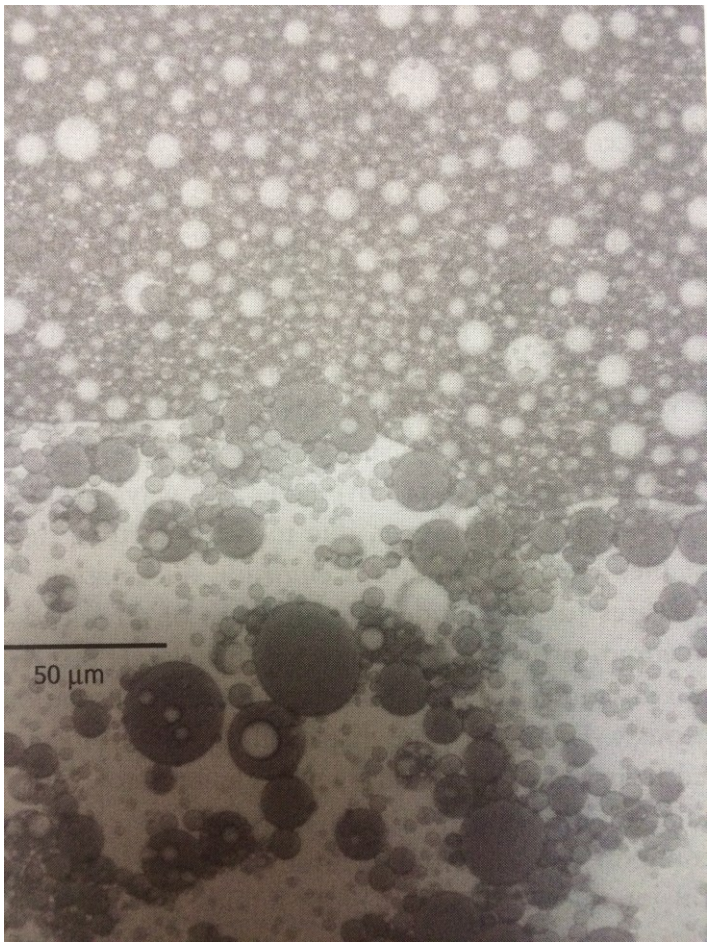

Figure 3 Photomicrograph of naphtha-diluted bitumen after centrifugation (Masliyah, Xu et al. 2011)

`

One of major challenges faced by oil sands industry is the consolidation of fine solids and clays in tailings pond to form sludge. The forces between the colloidal particles of the sludge become so strong that it doesn't allow for further settling and compaction. This leads to water laden sludge, containing 30% solids, 85% water and 2% unrecovered bitumen by weight, that eventually settles at the bottom of tailings pond for decades.

(Gray, Zhenghe et al. 2009) Presently, the total area of tailings pond is 170km^2. (CAPP 2011) Accumulation of sludge poses two problems: a) The ever-rising sludge demands for an increase in land. This would, in turn, disturb the ecology, b) Sludge is too fluidic to bear any weight. Solidification of sludge by removing water could help remediate the space for wildlife and vegetation. One approach made to make the sludge dense is by adding sufficient amount of gypsum (calcium sulfate) (Gray, Zhenghe et al. 2009)

While processing bitumen from oil sands, almost 90% of the bitumen is recovered. However, the remaining 10% of the bitumen along with a little fraction of naphtha is drained into the tailings. This leads to a significant loss of energy. (Camp 1976) A number of methods have been employed to recover the lost bitumen and naphtha in the tailings. These methods include flocculation, flotation scavenging, aeration and sorption put forth by a number of researchers. (Sengupta, Tollefson et al. 1997) A novel approach to recover residual bitumen and naphtha was suggested by Hudson and Sietzer in 1971 wherein they used sorption of bitumen and naphtha on oleophilic particles. (Hudson and Seitzer 1971) Oleophilic coke was used as a sorbent for recovery of 90% residual bitumen and solvent by contacting the tailings with coke either by bubble mixing, tumbling, shaking, stirring or using fixed beds. (Hall, Tollefson et al. 1988) In yet another effort, a fraction of tailings was sent to tails oil recovery unit before discharging the whole of residual bitumen and naphtha in tailings pond. This helped minimized bitumen and naphtha losses in the tailings. Tails oil recovery unit was installed by Syncrude Canada Ltd. (Cymbalisty, Cymerman et al. 1989) Steam stripping process was also used to recover a major quantity of naphtha lost to the tailings. (Clark et al 1988)

Of all the naphtha used in processing bitumen from oil sands, a small fraction, being less than 1%, is lost to tailings that cannot be recovered and becomes a part of mature fine tailings (MFT). (Siddique, Fedorak et al. 2007) For instance, Naphtha loss by Syncrude is .0043 bbl./bbl. (AERI 2008)

1.3 Objective of the thesis

The study has been motivated by current techniques used in oil sands industry for the analysis of naphtha incorporated into mature fine tailings. Obtaining a detailed composition data of tailings is essential for several purposes. Naphtha, comprising of olefins, paraffin, iso-paraffins, naphthenes and naphthenic acids leads to toxicity of tailings ponds. (Siddique, Fedorak et al. 2006) This renders harm to aquatic organism by penetrating through their cell membrane. (Quagraine, Peterson et al. 2005) In addition, it is also important to know the fraction of naphtha that is left unrecovered, to help prevent undue cost and energy losses.

Presently, a sample of mature fine tailings is collected and transported to laboratory every 6 hours to monitor its naphtha content using Gas Chromatography Mass Spectrometry. This method of detecting naphtha is time consuming, expensive and requires trained personnel. Above all, it does not allow for real-time detection of naphtha in the tailings.

In order to meet the demand of real-time naphtha detection in mature fine tailings, an approach for design and development of fluidic delivery line as processing unit for naphtha sensor has been made. In addition, the approach overcomes other disadvantages faced by current practices. The device would be miniature, inexpensive and potable. Furthermore, there would be no need for a trained personal to operate it.

1.4 Outline of thesis

Chapter 1 gives an overview of oil sands, its composition, formation and various techniques employed for bitumen extraction from oil sands. It also highlights main areas where oils sand deposits are found. A brief data is given for estimated bitumen production in coming years along with the by-product formed in its processibility. This chapter delineates the use of naphtha in bitumen extraction process and its occurrence in tailings. It describes various techniques used to reduce naphtha and residual bitumen lost in the tailings. It also states the objective of the thesis.

Chapter 2 discusses the literature review carried for to meet the research needs. This chapter flows into two parts. In the beginning, being main part of the thesis, delineates literature review carried towards designing of the mesofluidic delivery unit using the droplet system. The later part of the chapter talks briefly about the literature review conducted to propose a fluidic delivery unit that can be used for future work.

Chapter 3 delineates the experimental procedure and materials used in designing of the fluidic delivery unit. It describes step-by-step methods used in the making of different sub-units of the system.

Chapter 4 discusses on the experimental data drawn using the designed unit. In addition, it elaborates on the specifications and conditions for using the fluidic delivery system prepared to deliver feed to the sensor.

Chapter 5 highlights an approach made to design second model for Naphtha detection. It discusses work done thus far and also gives a relationship between pressure-volume for the proposed system.

Chapter 6 talks about the thesis in a nutshell. It also gives suggestions for future work.

Chapter 2 Literature Review

Environmental monitoring has become increasingly important in recent years due to increasing concerns over industrial and urban contamination with chemical and biochemical agents. A regular protocol for environmental monitoring involves collection of samples manually and transporting these samples to facilities equipped with instrumentation where trained personnel analyze them. These strategies provide accurate readings but readings on a real-time basis. Furthermore, a lot of expense is involved in transportation, storage and installation of the sophisticated instrumentation. (Diamond, Lau et al. 2008, Ramirez-Garcia, Baeza et al. 2008)

A fluidic system can broadly be categorized as an open or closed system. An open fluidic system doesn't allow recirculating and retaining the working fluid. On the other hand, a closed fluidic system has the working fluid flow multiple times by recirculating and retaining it along its framework. There are two things in common for all kinds of fluidic system:

i) Working fluid

Working fluid, that can be either a liquid or a gas, moves through connected tubings/pipes, connectors, pumps and other devices of the fluidic system.

ii) Pressure difference

Pressure difference creates a net force, to allow movement of fluids through the system. It facilitates either closing or opening of valves, pushing a piston, among others.

Of several different types of fluidic system, one essentially consist of four major components, viz.,

i) Filtration unit

ii) Pump

iii) Transition unit

iv) Collecting chamber

Filtration of feed is inevitable to make the working fluid devoid of any particulates and thus, prevent clogging of the system. Selection of pore size of filter membrane is system specific and depends on a couple of factors discussed in mid section of this chapter. Pump helps in moving the working fluid through the system. There are different types of

pump and based on one's application, its selection is made. With the advent of microfluidic technology, miniature pump are commercially available and fits into the system easily. However, fabricating pumps within the chip requires quite an effort and fineness. This is usually untaken in specialized fabrication laboratory with due care. Transition unit forms the central part of a fluidic system. There are several ways to transition working fluid to the fluid in desired phase. Furthermore, there are different modes of obtaining this transition of working fluid. To name a few, solvents are generally used along with the working fluid to obtain the desired fluid. These solvents tend to have high vapor pressure and thus, create the necessary pressure difference within the system to facilitate transition and flowing of the working fluid. Another way to have vaporized output fluid is heat. Heating the incoming working fluid to its desired temperature facilitates transition of liquid fluid to its vapor form. Creation of partial vacuum much to the vapor pressure of the working fluid can also provide the necessary transition. Collecting chamber is required to store in the incoming fluid from the transition unit for further analysis.

Lab-on-a-chip arrangements are used for the miniaturization of biochemical and chemical analysis. Manipulations of the analyte transport, characterization, separation and their detection are incorporated in a single platform of few centimeters. This leads to dramatic reduction in the amount of analyte used as well as on the time of detection. Furthermore, use of these arrangements also reduces cost than the "macro-laboratory" set-ups. In-situ analysis prevents human intervention, which in turn, reduces sample contamination possibilities.

Fluid handling in a system has several modes of ejection of the working fluid. This can be droplet-based or continuous throughput-based. In a droplet-based fluid handling system, the working fluid is obtained as drops at the outlet of the fluidic system. On the other hand, in a continuous throughput based fluidic system, the output working fluid is obtained in a continuous manner either in liquid phase or vapor phase, as demanded by the application. Droplet-based microfluidic systems are used in most applications. A few are detailed in mid part of literature review. In some cases, a mixture of gas and liquid can also be obtained at the outlet of the fluid handling system.

A miniaturized analysis system allows us to perform quick analysis of samples while reducing the sample amount, waste storage and power requirement. (Bowden, Sequeira et al. 2002) In addition to low power consumption and other advantages, the arrangement offers reliable information on the state of sample during its deployment period. (Bowden, Sequiera et al. 2002) Eutrophication of natural water manifested by algal bloom can result in toxicity of water, thus, rendering harm to aquatic animals and impairing the use of water for drinking and other purposes. Phosphate was found to be a significant element leading to its cause. (Carpenter, Caraco et al. 1998) It is of utmost importance to analyze water bodies of its phosphate content to keep its concentration under control. (Manuel 2014) Conventional way of water quality monitoring samples involved sampling, transport, storage and observation of protocols. (Jordan, Arnscheidt et al. 2005) To overcome significant manpower needed and high cost associated with the conventional techniques, John Cleary et al. developed a portable sensor for the analysis of phosphate in aqueous samples that incorporated microfluidic technology, wireless communication and calorimetric detection in a compact and potable devise. (Cleary, Slater et al. 2010). Of all the components of the analyzer, fluid handling was facilitated by a sample port to collect water sample that is to be analyzed, and an array of solenoid pumps were used to pump the water into the microfluidic chip wherein it is allowed to mix with a reagent before delivering to the photodiode and LED for detection purpose.

McGraw et al. made a similar approach for real-time phosphate detection in natural waters using microfluidic system. This system was based on yellow vanadomolybdophosphoric acid method for detecting phosphate. The current devise also incorporated filtration of the natural water, prior to phosphate detection, within the analysis system. Peristaltic pump was used to control the fluid flow into the microfluidic chip that bore a serpentine channel that facilitated solution and reagent flow designed in such a way that it covered all the active area of photodiode detector. Wireless communication allowed for real-time readings to be downloaded and saved in a remote land. (McGraw, Stitzel et al. 2007) Clearly et al successfully monitored phosphate levels in waters in Co. Dublin, Ireland in two deployment phases covering approximately 3 months, viz., September-November, 2009. This provided justification to the portable

detection devise designed much in the same manner as work conducted by McGraw et al. (2010, Cleary, Maher et al. 2010)

Besides successfully building miniaturized portable detection devises previously, there were a couple of technical constraints that were still unresolved. Stability of the reagent and power consumption in extreme remote environments were among the few. Works by Legiret et al. focused on eliminating such constraints to build devices that could be implemented in extreme conditions as well. The current portable devise used stable reagent, low reagent consumption and customized power cell for detecting phosphorus in both marine and freshwater environment. Various components used in building the devise were a customized syringe pump to pump in the liquid, valves, fluidic connectors, microfluidic chip that facilitated fluid flow within the channels cut through them, and data logging and control electronics that downloaded the real-time readings of phosphorus concentration in the liquid. The analytical method consisted of four phases: (1) intake of water sample from the source, (2) mixing of the sample with reagent in the microfluidic chip, (3) distinguished formation of color and (4) detection of phosphorous concentration by absorbance method. This devise has a potential to detect 10 samples per hour. (Legiret, Sieben et al. 2013)

Miniaturized systems were developed to detect nutrients and chemicals, other than phosphate in aquatic environments as well. Monitoring of nitrite levels became increasingly important to safeguard human health and to understand aquatic conditions in a better way. (Zazoua, Hnaien et al. 2009) Periodic knowledge of nitrite levels in water bodies is important, as nitrite is a by-product of phytoplankton as well as nutrient to the same. (Lomas and Lipschultz 2006) Unlike commercially available detectors to monitor nitrite, work conducted by Beaton et al. led into devising a miniaturized portable system to monitor nitrite. This analysis used low power and gave a high-integrated performance. Syringe pumps were used to drive the liquid through the delivery tubing into the Polymethylmethacrylate microfluidic chips for mixing of the withdrawn sample with the reagent. The fluidic manifold incorporated a polyethersulfone filter membrane to prevent the particulate matter from entering the system. Photodiodes were housed in customized electronic package that detected nitrite presence in the sample. This automated nitrite

monitoring system could operate for 57 hours while giving 375 discrete readings. (Beaton, Sieben et al. 2011)

Czugala et al. designed a wireless and portable microfluidic analysis system for quantitative measurements of nitrite in freshwater using Griess reagent. Griess reagent was prepared using N- (1-naphthyl) ethyenediamine dihydrochloride and sulfanic acid solution. To employ fluidic handling in micro- environment, photo-controlled polymer gel microvalve were incorporated in the microfluidic chip wherein mixing of the sample and reagent was allowed prior to its detection by the two diode set-ups. Current analysis system design could specifically be used for nitrite detection or chemical analyte by bringing in desirable changes in the set-up. However, due to release of photons in the surrounding 'gel' solution, a similar system cannot be used in biochemical analyte measurements. (Czugala, Fay et al. 2013)

In a comparative study conducted by Ziolkowski et al. on first and second generation of fluidic based chemical analyzers for monitoring nitrite, phosphate, pH, among many others, it was found that the cost of first generation analyzers were almost 7 times more that the cost involved in second generation analyzers. 50% of the total cost of analyzers was that of fluid handling systems. In first generation analyzer, fluidic handling, electronics package and housing accounted for 84%, 11% and 5% respectively, whilst, it was 63%, 11% and 26% in second-generation analyzer. (Ziolkowski, Czugala et al. 2012)

Of the various components used in the miniaturized set-up for monitoring analytes, micro pumps serve as one of the essential components. They help in flow controlled delivery of the samples that may range from flow rate as low as in microliters per minute to deciliters per minute. There are different types of micro pumps designed to meet different requirements. Woias et al. and Santiago et al classified the pumps based on their pressure and flow rate of the sample. They came up with two types of pumps, viz., displacement micro pumps that worked on discrete volume of fluid and continuous flow micro pumps that allowed fluid to flow continuously from the source. (2004, Woias 2005) Based on the working principle of the pumps, Nguyen and Wereley classified the pumps as mechanical and non-mechanical micro pumps. Non-mechanical pumps devoid use of any moving parts to provide momentum to the fluid. It converts any form of energy either in kinetic energy or pressure that facilitates flow of the fluid. On the

contrary, mechanical pumps uses moving parts to allow fluid flow. For instance, peristaltic pumps, viscous pumps, membrane pumps, among others are all mechanical pumps. (Nguyen and Wereley 2002) Mechanical pumps can be used in applications that demand high volumes of fluids. For instance, mechanical pumps are used in microelectronic systems in cooling of laptops. (Ma, Chen et al. 2009) On the other hand, non-mechanical pumps work well in most biochemical analyzers that require low volumes of fluid. (Nguyen and Wereley 2002)

Among the aforementioned pumps, Peristaltic pumps can be exclusively used for fluid handling. Peristalsis movement occurs when there is a contractile wave-like motion of the walls of a tube through which the liquid is flowing. This concept is used in both macro- and microenvironment. In macro peristaltic pumps, rollers are used that presses flexible tube containing the fluid against them. A continuous peristaltic transport of the fluid is obtained from these pumps. On the contrary, peristaltic transport of fluid in micro environment, viz. microfluidic chip, is conveyed by incorporating actuators or more likely known as pumping steps. (Berg, Anderson et al. 2003) Peristaltic micro pump uses no less than three actuators. (Nguyen and Huang 2001) Anderson et al. work on implementing 'two-stage' peristaltic pump showed that a comparable fluid flow rate can be obtained to the conventional 'three-stage' peristaltic pump. The current design of peristaltic pump gave low backpressure and reduced on chip design complexities and its area to 1/3 of the conventional counterparts. (Berg, Anderson et al. 2003) A novel approach on fabricating a peristaltic pump within a microfluidic chip using cascaded actuators was made by Jeong and Konishi. (Jeong and Konishi 2008) Lai and Folch provided further works on design and fabrication of peristaltic PDMS micro pump in a microchip. This design is expected to process fluid in a high throughput microfluidics. (Lai and Folch 2011)

Selection of pumps as per the application is important and requires careful evaluation. When selecting a pump for a fluidic delivery system, factors that must be taken into account are:

i) System operating pressure

ii) Expected length of service

iii) Desired flow rate in the system

iv) Environmental conditions

v) Cost of the pump

It is of utmost importance to consider system-operating pressure while selecting a pump. Low pressure would lead to dead end giving a static system where no working fluid would be able to flow. On the other hand, pressure above the threshold limit of the system would disrupt the system, possibly, leading to leakage in most cases. Desired operating pressure range as needed in the application should be taken into account and careful selection of pump to work under this pressure range should be made. Equally important is the time until which the pump would wear and loses its efficiency to work any further. Length of service of the pump, thus, should not be neglected if we have to run r the system for long duration, in particular. Pump can either provide constant or variable output response and depending on the application, selection is made for either constant or variable pump. A constant flow rate pump gives an equal output fluid per unit time. On the other hand, variable pumps have different flow rate of working fluid. There are pumps that have different flow rates in their frame and depending on the desired flow rate in the system, a particular flow rate can be marked. Despite of all the possible flow rate options in the pump, the pump would give a constant flow rate that has been marked. Environment can play an important role in the selection of pump as well. A sturdier framework of pump would be encouraged for a system operating in harsh environment. There is a likeliness of the pump cover to damage in environment bearing extreme temperatures, pressure, among others. The shell enclosing the pump system should be both physically inert to wear and tear and chemically inert to corrosion or any reaction with substances present in environment. Furthermore, the nature of working fluid also should be considered in pump selection. Presence of highly reactive chemicals in working fluid is likely to eat away the walls of pump within a short span. Viscosity of the fluid also determines its flow through the pump. A more viscous liquid would demand the pump to perform more work to make it flow in the tubing. Pressure to push/pull a highly viscous working fluid is high and thus, it is advisable to select pumps that have a higher operating pressure range. Nature of pump framework and feed characteristic is thus necessary in pump selection. Lastly, cost of the pump can never be taken for granted.

For a more commercial fluidic system, cost is inevitable. A low cost fluidic system providing good output response is mostly demanded.

Microfiltration is one of the first filtration processes developed in the year 1929 in Germany. There were predominantly made of nitrocellulose until 1963. However, with the advent of emerging chemical and biochemical processes, improvements have been made in terms of material selection and chemical resistance based on their usage in different applications, viz., water purification, microbiological and similar other analytical applications.

Membrane filtration is one of the most economical ways of separating particulates present in a liquid. This membrane generally has two layers, viz., a porous supporting layer and a dense porous layer that is customized based on one's application. This membrane acts a physical barrier wherein particulates larger than the pore size are retained on the incoming fluid end of the membrane, thus, allowing the filtrate to pass to the other end. Report by Ahsan Munir describes different types of membrane filtration. They are described in a nutshell as given below:

i) Ultrafiltration

This type of filtration is used to separate extremely small molecules or particulates from a fluid. Pore size of the membrane is generally based on the size of the molecule/particulate in interest. However, Molecules/ particulates having same size cannot be separated individually. In addition, ultrafiltration can also retain coarser components of the fluid. Average pore size of membrane filter used in ultrafiltration is generally 0.01μm. It is exclusively used in removal of molecules having low molecular weight, viz., proteins.

ii) Microfiltration

Particles or entities with a size ranging from 0.025 μm to 10.0 μm can be effectively separated from the fluid using Microfiltration. The retention of particulates/entities by the membrane defines the efficiency of the system. In some cases, such a retention means can also be used for analysis purposes. For instance, retention of bacteria on the membrane for culture purposes.

iii) Reverse Osmosis

This type of filtration works at a relatively high pressure wherein; salts and molecules of interest are separated from their low molecular weight solutes. This molecular weight is usually less than 100 Daltons. For instance, reverse osmosis is used for purification of tap water.

iv) Cross-flow Filtration

This type of filtration does not allow retention of entities on the membrane due to turbulent flow of the flowing feed. Filter membrane is usually lined on the walls of the tube/pipe through which the fluid flow. In such a case, the high pressure flowing fluid washes off the retained particulates. The filtration direction is perpendicular to the fluid flowing through the tube/pipe.

v) Dead-end Filtration

This forms the basic form of filtration wherein, feed is passed through the membrane and the particulates gets accumulated on the incoming feed side of the membrane. With time, clogging of the filter membranes reduces filtration efficiency and demands either a backwash or replacement of the membrane. It also proves helpful in concentration of particles of interest.

vi) Submerged Filtration

In this type of filtration the filter membrane is completely submerged into the liquid that has to be filtered. Liquid passes through the membrane due to partial vacuum creation on the inside volume of the submerged membrane. The filtrate is pulled out from this space while the particulates retain on the outer surface of the filter membrane.

vii) Hybrid flow Filtration

This type of filtration comes includes both the dead-end filtration and cross filtration. The tubes/pipes perform two functions in one cycle of hybrid filtration, viz., production and flush. In production, the particulates are retained in the inside of the walls of tubes/pipes lined with filter membrane by closing one of its ends. Flushing wherein, the retained particulars are forced out to clear the filter space for another cycle of Hybrid flow filtration follows this.

Cross-flow microfiltration is a pressure driven filtration process that is generally used to remove coarse particulates and bacteria as well as smaller class of biological species that may range in Nano scales. Operating pressure for cross flow filtration usually ranges

from 0.1-8 bars. (Merin and Daufin 1990) Cross flow filtration is also known as tangential flow filtration. Works by Kim et al. uses cross flow filtration to harvest microalgae. The pore size of the membranes used in their works was 0.45μm and 0.2μm for different set of microalgae species respectively. (Kang, Kim et al. 2015) Presently, Micro filters are commercially available by several manufacturers in different forms and sizes. Based on the application, selection of the membrane with most suitable configuration is essential.

Micro filters are versatile to use, however, there are many bottlenecks that one faces overtime. Depending on the feed stream, fluid components, relative filter membrane pore size and high flux of the fluid passing through the membrane, there is a possibility of large particles or aggregates to clog the pores of the membrane that leads to the formation of filter cake. Overall characteristics of filtration are, thus, governed by the formation of filter cake and their properties. (Merin and Daufin 1990) Researchers have found that most of the rejection of membranes is mainly due to size exclusion and electrostatic interactions of the fluid particles and the membrane. (Yaroshchuk 2008) Several challenges that one faces while using membranes are formation of cake; commonly called fouling, transport description of the fluid containing complex mixtures and maintenance of large pressure gradients to pump the fluid across the membrane. Membrane technology has upgraded materials used in membranes to make them flexible, resistant to fouling and more cost effective. (Zhang, Zhao et al. 2014) Fouling of membrane can be either internal or external in nature. External fouling is largely due to particulates settling on the filter cake while internal fouling occurs when particulates get trapped in the pores or gets adsorbed in a way to partially clog the pores. Therefore, pore size of the membrane and particle sizes in feed is important in deciding the extent and nature of fouling of the membrane. (Liu and Sun 2012, Aslam, Lee et al. 2015) Most of the miniaturized analytical system developed for monitoring chemical and biochemical analytes used membranes with pore sizes ranging from 0.25 μm to 0.45 μm. (McGraw, Stitzel et al. 2007, Cleary, Maher et al. 2010, Cleary, Slater et al. 2010, Ei, MarineInstitute et al. 2011)

Blocking filtration laws describes mechanism of fouling of membranes first explained by Hermans and Bredee (Wang and Tarabara 2008) :

(a) Pore sealing: Pores are completely blocked by a seal, thereby, preventing fluid to flow through them. This seal reduces the membrane area open to fluid flow.
(b) Intermediate blocking: Blocking of the pore by the assumed seal resulted by fraction of particles and deposition of other particles on top of them.
(c) Cake filtration: Hydraulic resistance to filtration increases with the accumulation of particles at the surface of filter cake.
(d) Pore constriction: Membrane permeability is reduced due to accumulation of particles against the pore walls of the membrane.
Hermans described four mechanisms of fouling, namely- complete blocking, intermediate blocking, cake filtration and standard blocking by a power-law expression. (1982)

$$\frac{d^2t}{dV^2} = k\left(\frac{dt}{dV}\right)^n \tag{2.1}$$

Where,
V is the filtrate volume accumulated on the membrane
k is a constant
t is the filtration time
n is the blocking index, which is 0, 1, 1.5, and 2 for Cake filtration, intermediate blocking, standard blocking and complete blocking respectively. The mechanisms exhibited by aforementioned four types of membrane fouling are pictorially shown in figure 4 (Aslam, Lee et al. 2015).

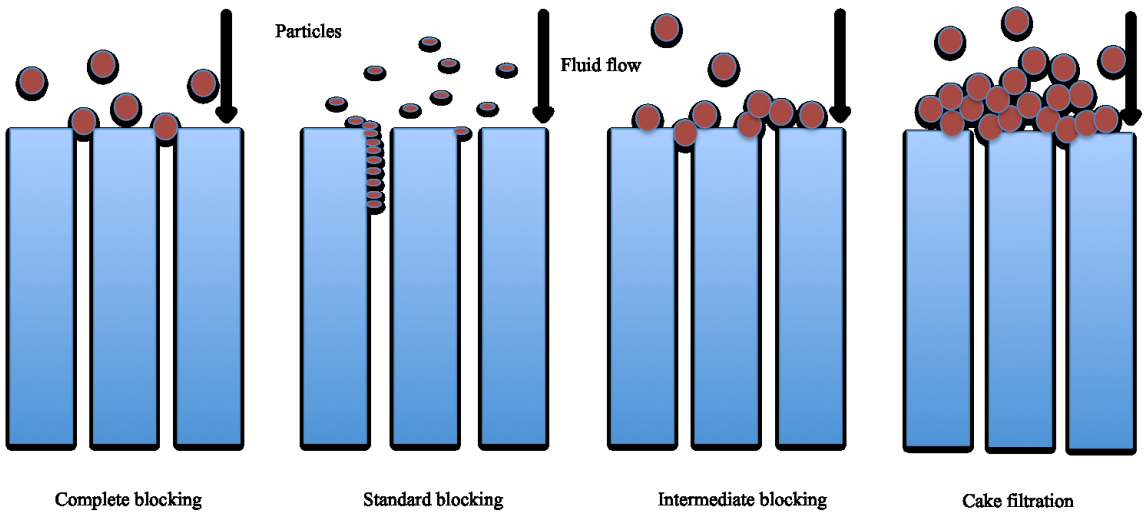

Figure 4 Schematic illustration of membrane fouling mechanisms described by four models

Hagen-Poiseuille Equation is generally used to understand the flow of liquid past a filter membrane in a dead-end filtration. This equation usually assumes membrane to have pores that are cylindrical in structure and parallel to one another. The flux through the membrane is then given by Hagen-Poiseuille as

$$J = \left(\frac{\varepsilon_m r^2}{8\eta\tau}\right)\left(\frac{\Delta P}{\Delta X_m}\right) \tag{2.2}$$

Where,

J is the flux through the filter membrane

η is the viscosity of the feed

ε_m is the porosity of the filter membrane

ΔX_m is the filter membrane thickness

ΔP is the pressure difference

Films are ubiquitous and play a crucial role in everyday processes. The study of dynamics and heat and mass exchanges in fluid films is necessary to understand these processes in a better way. Study of fluid films finds wide application in chemical industries, heat exchangers, and refrigeration, among others. Several researches have been made on the study of fluid films in heated environments.

The interaction of mechanism that affects the dynamics and stability of non-uniformly heated fluid films is detailed both numerically and experimentally. (Kabov 2010) Surtaev and Pavlenko made study on transient heat transfer in a falling liquid film. They showed stepwise generation of heat within the liquid film. At the place of vapor bubble formation on the heater surface, there is a decrease in temperature in the area above which nucleation occurs. A local increase in heat transfer intensity was shown in the same area. So-called temperature waves were formed at the free surface of the liquid film at the same time. (Surtaev and Pavlenko 2014) Petkovsek et al extensively studied temperature variation underneath the areas of growing bubble. They recorded the transient wall temperature using high-speed infrared camera and video to study movement of bubble. (Golobic, Petkovsek et al. 2009) Boiling of fluid film is determined by heat flux. When critical heat flux is reached, fluid gets separated, either partially or completely, from the heating surface. This leads to decrease in heat transfer intensity and subsequently, increases the temperature of the same area. (Surtaev and Pavlenko 2014)

Gupta et al conducted fluid flow analysis and particle transport within a droplet exposed to external radiation. They have shown how change in free surface temperature could alter fluid profile in the droplet. (Thokchom, Gupta et al. 2014)

With the advent of microfluidic technologies, incorporating micro heaters, micro pumps, and membranes, among others, within the chip, can facilitate change of fluid from liquid to vapor phase in much smaller footprint. Bentley et al. presented a way of programming fluid flow in microfluidic networks using evaporation. A microfluidic network typically consists of open port to fill the fluid, sealed microchannels and an open capillary pump. The arrangement focuses on ultra low flow rates in microfluidic chips and works by (a) controlling the evaporation rate and, (b) preventing undesirable evaporation elsewhere. (Zimmermann, Bentley et al. 2005) Despite several researches done on the microfluidic networks and passive controlled pumping of fluid using evaporation, none could determine a stable fluid flow over an extended period of time. Lynn and Dandy designed a microfluidic chip in which large pressure differential drives the fluid to flow through the microfluidic channels. This passive continuous pumping system finds application in Lap-on-a-chip devices that exhibits pressure driven flows. (Lynn and Dandy 2009) Davoust and Theisen determined evaporation rate of drops in

microsystem. Impact on drop evaporation of different configuration of drops was studied. (Davoust and Theisen 2013) Becker et al. fabricated an evaporation induced flow in a microfluidic chip exhibiting capillary driven fluid flow. The current chip enhouses micro heater that gets actuated upon complete filling of the capillary with the fluid. A high flow rate of 8 nL/s was found by capillarity and evaporation induced flow. (Gray, Becker et al. 2014)

A widely known model of evaporation assumes a half-spherical water droplet with radius R=R(t), with R_0 as its initial value. Evaporation is acting to reduce the radius of the droplet inward. Picknett and Bexon gave an expression to such a model with constant contact angle. (Picknett and Bexon 1977)

$$R(t)^2 = R_o^2 \left(1 - \frac{t}{\tau_{evap}}\right) \tag{2.3}$$

Where,

$\tau_{evap} = \frac{R_o^2}{4D_{vap}(C_0 - C_\infty)}$ ρ is the characteristic evaporation time scale

ρ is the density of water

D_{vap} is the diffusion coefficient of water vapor

C_0, C_∞ are mass concentrations in water vapor at the interface and further away from it.

Kobayashi and Konishi implemented a novel microfluidic structure. In the current arrangement, three polydimethysiloxane (PDMS) layers were heat sealed into one chip to improve biological blood separation. Filter membrane with ultra small pores of 0.4 μm diameter was sandwiched between the upper and lower corrugated sheets to obtain purified blood in all the cubicles. Filter membrane was polycarbonate-type filter. Fabrication of this novel design was cost effective and has the potential to be implemented for μTAS applications. (Kobayashi and Konishi 2012)

Presently, most of the applications use power supply, either directly or indirectly. It is a device that converts one form of electrical energy to another. Power supplies have varied designs and uses. Based on their functional means, they can broadly be categorized as

i) Regulated power supply

ii) Adjustable power supply

iii) Adjustable regulated power supply

iv) Isolated power supply

Regulated power supply is one in which the output voltage or current remains constant to the varying input voltage. Adjustable power supply is one that has means to adjust the output voltage or current, which may be either by an outer knob or by changing the input voltage. Furthermore, an adjustable regulated power supply combines the power supply mentioned previously to give a regulated voltage or current with adjustable input. An isolated power supply gives output voltage or current that does not depend on the input.

A well-known classification of power supply is DC power supply and AC power supply. Direct current power supply essentially uses a voltage having a particular polarity to be transmitted to its load. On the other hand, an AC power supply gives the desired output voltage or current by withdrawing the voltage from the main board and stepping down to the desired destination. Furthermore, an AC power adapter is one in which AC main work frame is enclosed.

Knowledge on properties of materials to fabricate the microfluidic chip is essential. Feed suspension, flow rate, heated/non-heated environment, among others plays a vital role for selection of materials. Initially, glass was primarily used for fabricating microfluidic chips. However, with extensive researches in material science and engineering, there is wide variety of materials to choose from depending on the specific application. Becker and Locascio give a tabulation enlisting important properties of widely used materials for microfluidic chip fabrication, viz., polymethymethacrylate, polycarbonate, polyethylene tere-phthalate glycol, polyethylene, polyimide, styrene copolymer and silicone. (Becker and Locascio 2002)

Wax bonding process is used lately for sealing of different layers of chip material. It is cost effective, easy to fabricate and adheres between the layers in short span of time. The wax is sandwiched between the layers and allowed to sit for sometime. Melting then pumps unwanted wax out. Furthermore, wax is reusable and its bonding process can be reversible by melting and cooling. An alternative way to seal these layers can also be done by using acrylic glue which holds its own benefits, viz., it’s easy to apply between

the sheets, low cost and adheres rapidly. However, it is not reusable. (Gong, Yi et al. 2010) Works by Diaz-Gonzalez and Baldi also uses low temperature wax bonding to fabricate biofunctionalised microfluidic framework. (Díaz-González and Baldi 2012)

One of the major challenges faced in lab-on-chip devices is the movement of samples from macro environment to micro one, viz., world to chip interface. Compression seals fittings were used to introduce sample into the chip. These interconnects are based on interlocking, self-aligning, mechanical bonding and photo patterned silicone O-rings. However, these interconnects do not guarantee leak proof environment under high pressure driven flows. (Gonzalez, Collins et al. 1998) Much research has been made in microfluidic interconnect to build a robust design that could meet such challenges. Leak tight interconnects have been designed overtime. They are robust and can withstand high pressure but are not cost effective, as it requires substantial effort to build. Advent of 3D printing technology can help ease machining these robust microfluidic interconnect at an affordable cost. They are customizable and more reliable. Paredes et al. machined first 3D printed microfluidic interconnects. Recently, 3D printing has also allowed combining rigid and soft polymers together in a single run. One of the major advantages of 3D printing interconnects is that both gasket and clamps are fabricated in a single run. Current interconnect works effectively under high pressure and has an extended length of service. (Paydar, Paredes et al. 2014)

As discussed already, pumping is essential to transport sample in microfluidic set-ups. Of several other categories of classification, pumps can be either on-device or external in nature. External pumps are located outside the microfluidic chips while on-device pumps are incorporated within the chip volume. Despite of low footprint in the latter, it comes with complexities in its fabrication, which in turn, increases cost. Furthermore, they are fabricated to be disposable in nature to avoid contamination of the sample induced in it. In this case, external pumps become an attractive choice. However, it would be even more beneficial in remote environments if very or no power consumption was needed. There are several external pumps to choose from, viz., syringe pumping, electro-osmotic pumping, among others. Chien et al. devised a simple pump that is capable to generating either positive or negative pressure for driving fluids in microfluidic applications. It works by changing the volume of air confined within the closed set-up and is also

capable of generating vacuum. This current system is cost effective and does not require any power consumption. An expression was generated for this model that helped finding the gauge pressure of the system. Operating pressure that could be generated with this low dead volume pump ranges between -95 kPa to 300 kPa with a high resolution of 1Pa. It can provide continuous flow rates and it highly pressure-sensitive. There is a potential for this system to find application in stimulation of cells mechanically. (Moscovici, Chien et al. 2010)

Microfluidic technologies have open up a new platform for several analytical applications. Conventional monitoring system is shrinking gradually to a mesoscale, microscale or nanoscale footprint. Lot of improvements has been made in last few decades. However, there is still room to optimize analytical system designs to meet the challenges being faced lately. Fluid handling at micro/meso scale is challenging yet it is highly cost effective. Efforts are to be made to have a fluidic handling system at meso or much smaller scale for commercial purposes. More specifically, microfluidic technology has an immense potential to find a wide application in oil sands industry in near future.

Chapter 3 Materials and Methods

3.1 Sample procurement

Oil Sands Innovation, University of Alberta provided sample used in the research. It is processed water containing naphtha that was collected from Syncrude Tailing Ponds.

3.2 Wireframe outline of fluidic delivery line for Naphtha detection

The wireframe design of fluidic delivery line for Naphtha detection is shown in figure 5.

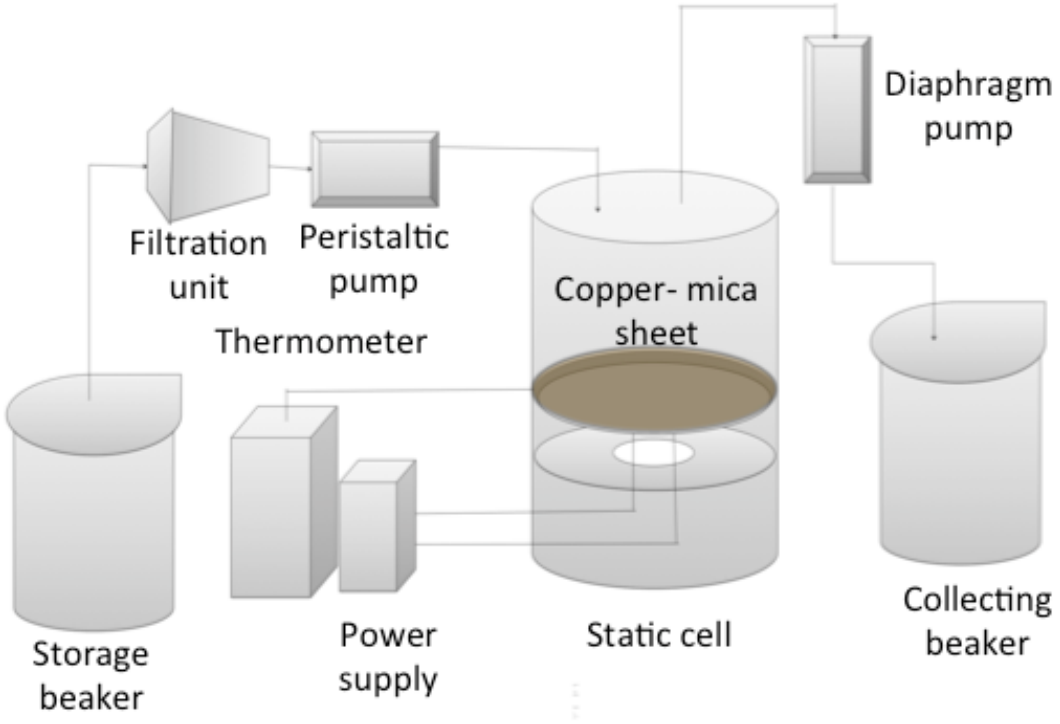

Figure 5 Wireframe outline of fluidic delivery line for Naphtha detection

The fluidic delivery system consist of various components which are as enlisted below:

(a) Filtration unit to collect and filter the sample

(b) Peristaltic pump

(c) Polytetrafluoroethylene static cell

(d) Plate of copper and mica sheet pressed together using Teflon tape

(e) Customized nichrome design

(f) Micro diaphragm pump

(g) D.C. power supply

(h) Reusable glass beaker as storage and collection chamber

(i) Silicone tubing to form connections between aforementioned components.

An open set-up containing aforementioned parts in its initial installation and their details are shown in figure 6. Fluke thermometer was used to check the temperature of the sandwiched plate by adjusting the desirable voltage of D.C. power supply. However, the final delivery arrangement does not include the thermometer as well as the power supply, which is alternated by D.C. batteries joined in series/ parallel according to the voltage needed by the heating unit.

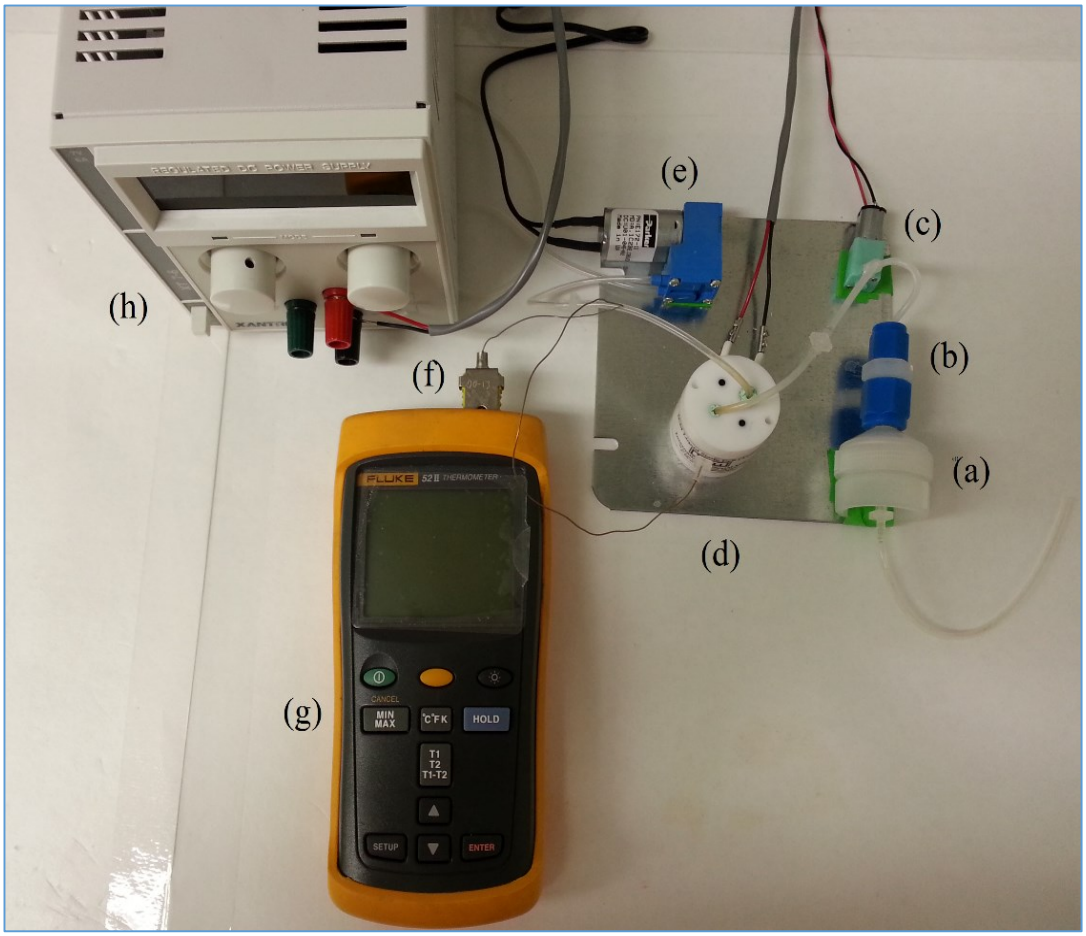

Figure 6 Experimental parts details (a) Filtration unit (b) Reducing union to connect filter holder to the pump (c) Peristaltic pump (d) Static cell enclosing heating system and platform for copper-mica arrangement (f) Thermocouple (g) Fluke thermometer

3.3 Filtration system

The miniature pumps-namely- Dolomite peristaltic pump (3200243, Dolomite Center Ltd., Charlestown, MA) producing a flow rate of 0.45ml/ min and Parker E172-13 BTC miniature diaphragm pump (Parker Hannifin corporation, Mooresville, USA) running with a flow rate of 6 slpm were driven by CUI EPS030100 3V power supply (CUI Inc., USA). The former helped pull in the sample from the storage beaker into Millipore Swinnex® filter membrane holder SX0002500 (22 mm diameter, 37 mm length) enclosing Millipore nylon filter membrane HNWP02500 with a nominal pore size of 0.45 μm and 25 mm diameter. This pore size was chosen as most analytical system uses a filter membrane with a pore size ranging from 0.45 μm to 0.2 μm as discussed in literature review. The latter pump delivers vaporized sample into the collection beaker. The filtrate would represent the real system.

3.4 Miniature heating unit

A miniature heating system is designed to contain inside static cell (International Crystal Mfg., Oklahoma, USA). Nichrome wire of 4.75 ohm/ft. (NW28500, Jacob online) was chosen to heat a united plate of circular copper sheet (300599754785, 19 mm diameter, 1.30 mm thickness) and circular high temperature mica sheet (320675508117, 19 mm diameter, 0.20 mm thickness) using Teflon tape (151225216573). The arrangement is heated with a D.C. power supply (XT 7-6, Xantrex, USA) at 3V 2A. Dolomite silicone tubings (3200173, Dolomite Center Ltd., Charlestown, MA) were used to connect different components with the help of polypropylene barbed union material.

3.5 Working of the delivery system

Processed water is made devoid of any particulate matter in filtration unit before running down through the peristaltic pump into the static cell. This is done to avoid clogging in the system. Nichrome wire coiled spirally and encased in ceramic tubes (TRM-04018-12, Omega, Canada) is fixed at the bottom of static cell. Adjusting the

output voltage of D.C. power supply to 2A 3V facilitates heating of the wire. Winding Teflon tape at its periphery held circular copper sheet and mica. The arrangement was placed on the spiral nichrome wire using 7548A11 heat transfer epoxy with copper facing the incoming drops of filtered processed water. Omega KMQSS020G12 thermocouple (0.02 inch diameter) is sandwiched between the two sheets to measure the temperature. Reading of temperature is measured using Fluke 52II thermometer. Momentive RTV 106 Silicone sealant is used to seal any openings in the static cell.

The processed water gets vaporised after being dropped on the hot copper sheet. The vapors are pulled by miniature diaphragm pump into the collection chamber enclosing micro cantilever sensor that detects naphtha concentration in the sample. Working of the delivery system is illustrated in figure 7.

Analysis of the sample in terms of pH, particle size and concentration were made which is discussed in later section of this chapter. Furthermore, efficiency of the membrane filter to be used before complete clogging is also discussed alongside.

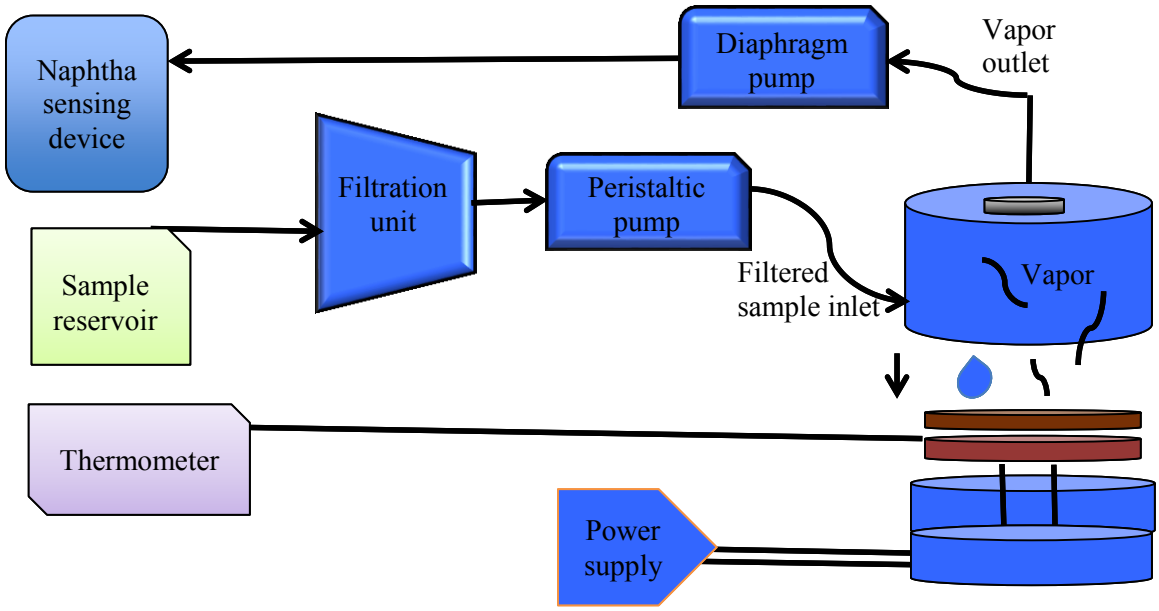

Figure 7 Schematic illustration of working of delivery system

Particle size measurement of particulates contained in processed water before and after filtration of the sample using membrane filter with 0.45 μm pore size was taken with Mastersizer 2000. The equipment was calibrated assuming Kaolinite to be predominant in the sample. Additional settings included Particle absorption index as 0.100, dispersant refractive index as 1.33, particle refractive index as 1.570 with laser obscuration ranges between 4.5- 13.58 %. The equipment performed 5 measurements at varying laser obscuration.

Varian Cary 50 Bio UV/ Visible spectrophotometer was used to measure concentration of particulates in filtered and unfiltered processed water. pH of both the samples was measured with pH meter (XL 20, Accumet Excel).

Correlation between mass filtrate and time was studied using Mettler Toledo XP203S to find the efficiency of the membrane filter to be used before clogging. A constant flow rate of 0.45ml/ min was maintained throughout the experimental run. This flow rate gave 11 drops per minute, ideal for the heated copper plate to vaporize the whole of the sample that was dropped to it. A higher flow rate would form a pool of droplets making vapor formation is a little time taking, whereas, a low rate is expected to cause loss of heat, among others.

Chapter 4 Results and Discussion

4.1 Real view of fluidic delivery system

A fully assembled delivery system could comfortably fit in a box of dimension 10 cm*13cm*8cm (width*length*height). Figure 8 shows the real view of the fluidic delivery arrangement. The heating unit is contained inside the static cell, which cannot be seen in the figure. Beaker with the black lid acts as a sample or more specifically, naphtha containing sample reservoir. In industrial application, this reservoir would scale to either tailing ponds or any other sources where naphtha needs to be detected.

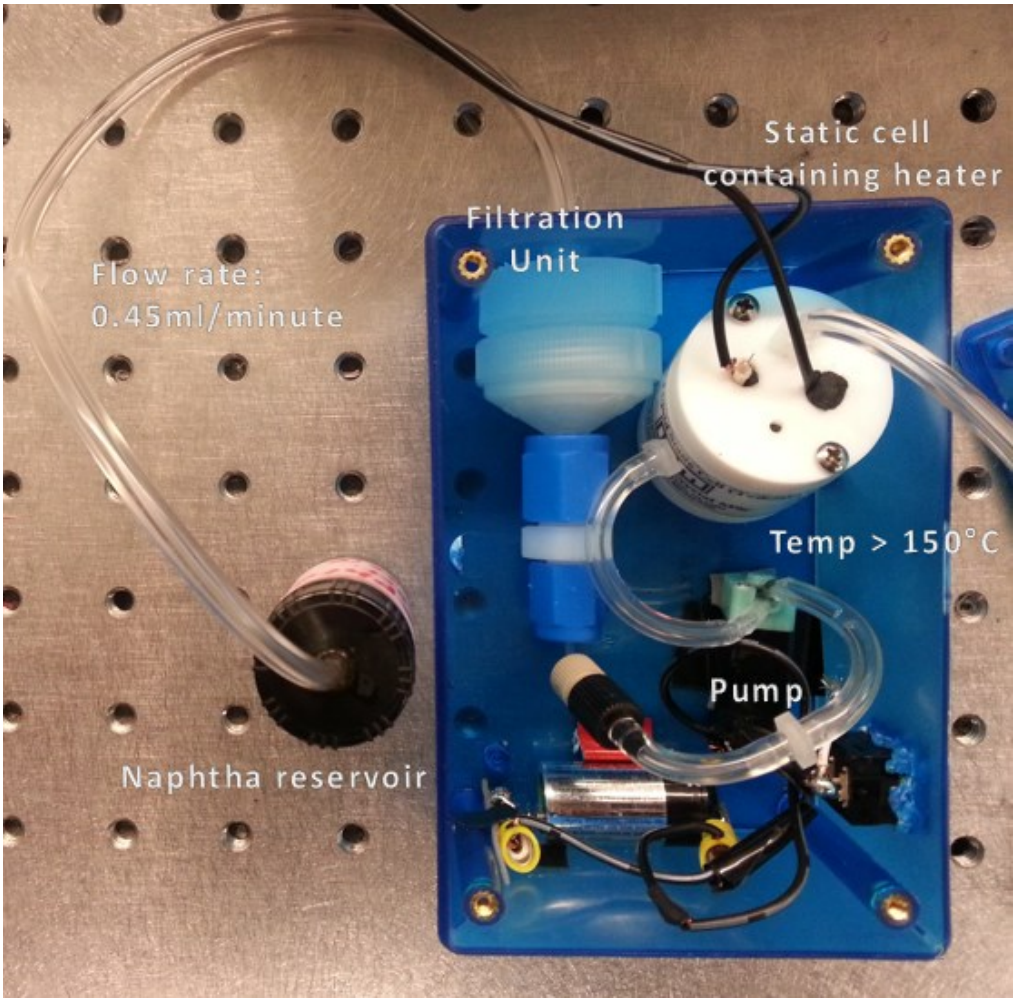

Figure 8 Real view of fluidic delivery arrangement

4.2 Filtration unit output as a function of mass filtrate per unit time

Filtration unit output as a function of mass filtrate per unit time is shown in Figure 9 At a constant flow rate of 0.45ml/ min, the membrane filter was found fully clogged after 3 hours 2 minutes. It took 12 minutes for the inlet tubing to discharge first drop of processed water to the measuring plate. In real picture, this measuring plate would be the copper sheet forming the accepting plate of heating unit. Figure 9 shows that there was good agreement between masses of filtrate with time until particulate obstruction resulting in slight rupture of membrane filter at 182th minute. From this time onwards, the data became erratic leading to termination of trial of membrane filter longevity.

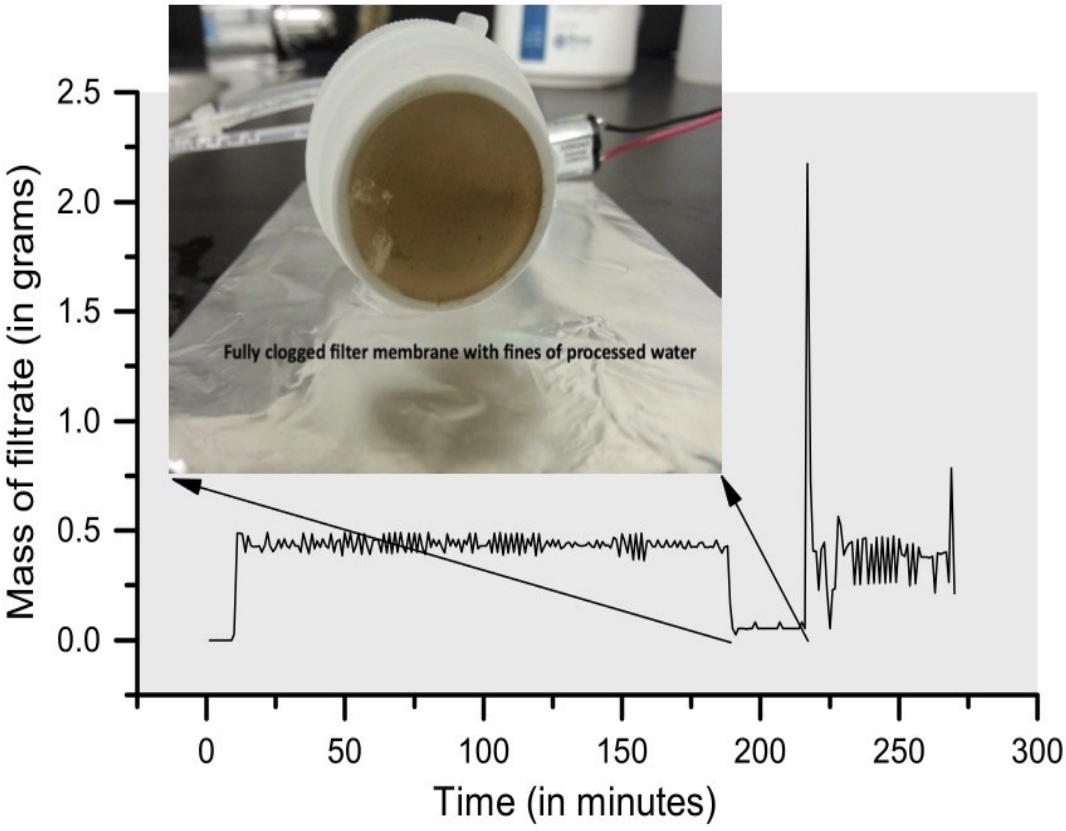

Figure 9 Filtration unit output as a function of mass filtrate per unit time

It should be noted that filter cake does not necessarily take the same appearance as shown in figure 9. Filter cake largely depends on the particulates present in the fed sample over the analytical time run. This trial period is for the sample that was provided by Oil Sands Innovation, University of Alberta. Mass of filtrate and respective flow rate of the sample with time is plotted in figure 10. Fluctuations in the flow rate of the sample flowing out of the membrane filter holder is dependent on the filter cake thickness and its configuration on the membrane interface. From the data obtained for the processed water, it is advisable to change the membrane filter contained in the filter holder after running the system continuously for 3 hours 2 minutes. Filter holder has a simple structure and opens with ease for membrane filter replacement.

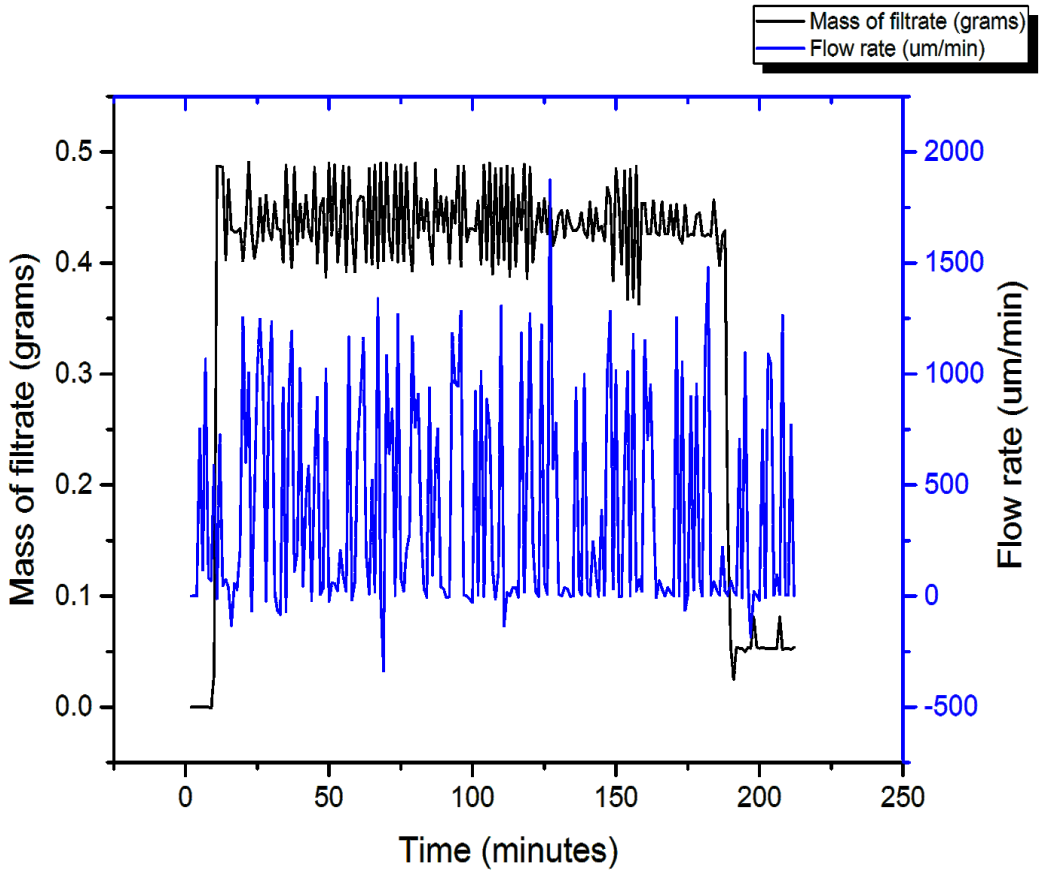

Figure 10 Plot for mass of filtrate and respective flow rate of the sample with time

4.3 pH of unfiltered and unfiltered sample

pH of the samples was measured with pH meter (XL 20, Accumet Excel). pH of unfiltered and filtered processed water was found to be 8.36 and 8.92 respectively. This shows processed water sample to be more of alkaline in nature.

4.4 Distribution of particle sizes and its respective volume density

Distribution of particle sizes and its respective volume density in unfiltered processed water is shown in figure 11. Maximum volume density was shown for particles with size 12.7μm. However, minimum volume density, viz. 0.01%, was found for particle size of 186 μm. As for particle size in a filtered sample, the lower limit of the measuring equipment, viz., Mastersizer 2000, prevented measuring size of particles, if any, that persisted even after filtration. However, deposition of any kind was not observed on the copper sheet for a trial run of 3 hours. A subsequent observation shows that there is a likelihood of almost nil or merger amount of particulates presence after filtration. The results obtained above show a viable way of using filtration unit with membrane filter of 0.45 μm pore size for the given processed water.

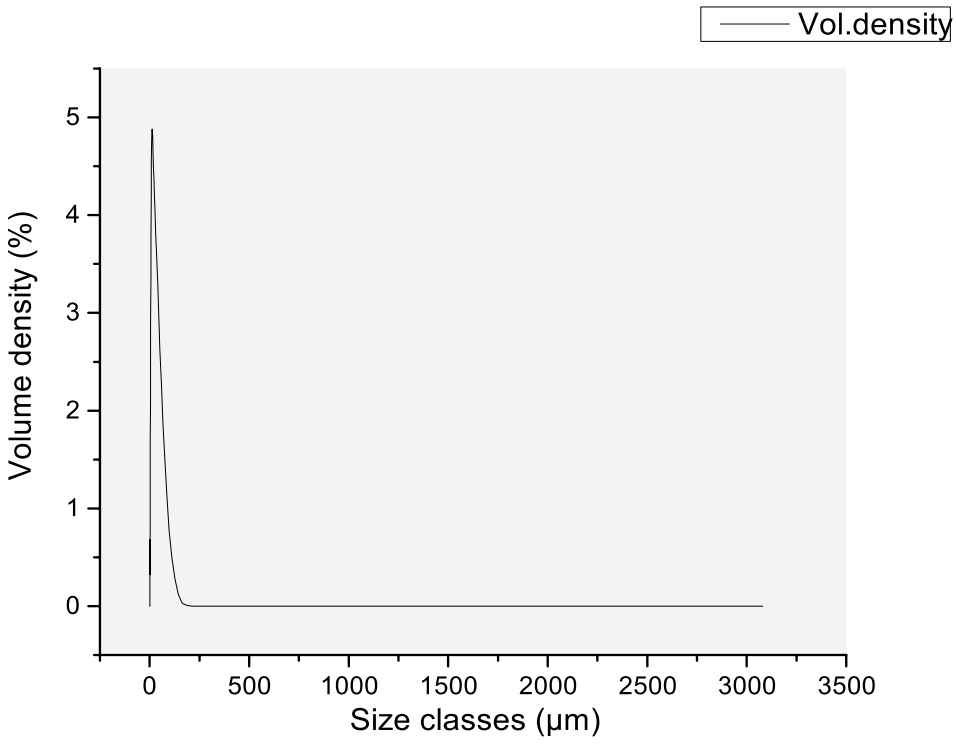

Figure 11 Distribution of particle sizes and its respective volume density in unfiltered processed water

4.5 Concentration of the sample

Figure 12 shows absorption spectrum of filtered and unfiltered processed water plotted as a function of absorbance with varying wavelength. Maximum absorbance for filtered and unfiltered sample was seen at a wavelength of 210 nm and 220 nm respectively.

Monochromatic radiation of power P was radiated at the sample contained in the cuvette in Varian Cary 50 Bio UV/ Visible spectrophotometer**.** Assuming the radiant power of beam of radiation leaving the sample to be $P_{i,}$ the amount of absorbance can be determined by the expression

Absorbance A,

$$A = \log_{10} \frac{P}{P_1} \tag{4.1}$$

Also, transmittance T can be expressed as

$$\%\mathrm{T} = 100\frac{P_1}{P} \tag{4.2}$$

Thus, $A = 2 - \log_{10} \%T$ (4.3)

According to Beer-Lambert Law,

$$A = \epsilon bc \tag{4.4}$$

Where, A is the absorbance, ϵ is the molar absorptivity in L/(mol.cm), b is the path length of the sample in cm, viz., path length of cuvette containing sample and c is the concentration of the sample in mol/L. More concentrated a solution is, more would be the absorbance as there will be presence of more molecules and ions to absorb the light. Depending upon the calibration of the spectrophotometer, a similar graph was obtained for both filtered amd unfiltered sample.

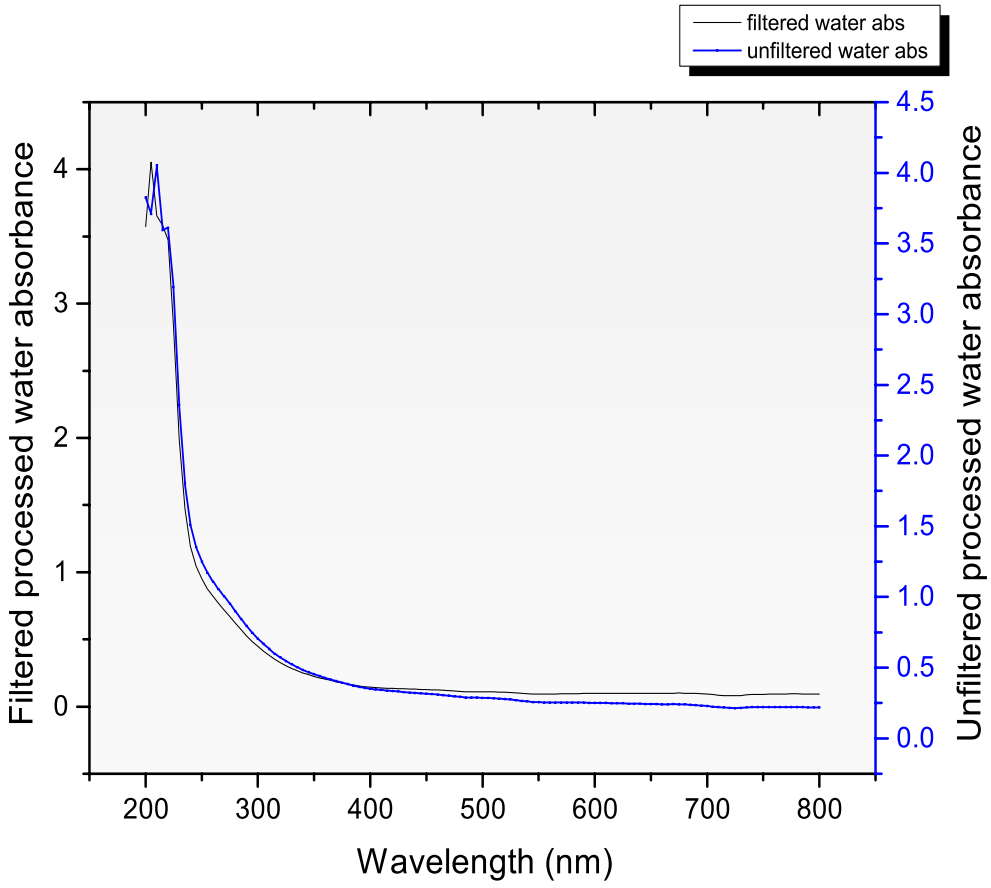

Figure 12 Ultraviolet/ visible spectrum of filtered and unfiltered processed water showing vibrational fine structure

4.6 Fluctuations in flow rate of the sample

Flow of fluid past the filtration unit is affected by several factors, viz., filter cake formation, its configuration and thickness, size of particulates entering the feed tubing, efficiency of the pump driving the fluid in and out of the unit, temporary accumulation of aggregates into the tubing rendering smaller cross sectional for fluid to flow, among others. Figure 13 shows fluid flow before entering the filtration unit and the different ways particulates can appear during its transit.

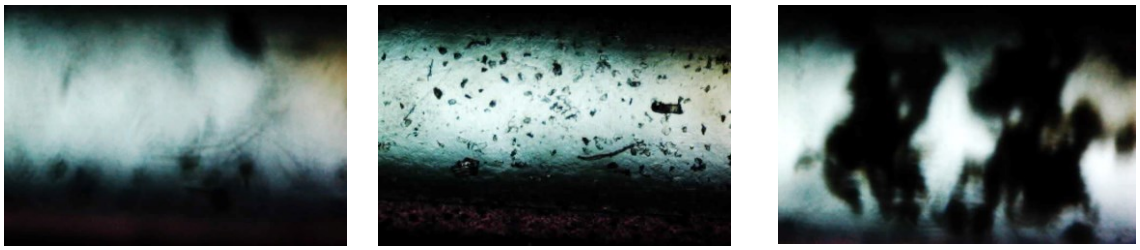

(a) (b) (c)

Figure 13 Fluid flow before entering the filtration unit (a) Scanty particulates in transit (b) Fine particulates in transit (c) Coarse particulates covering most cross sectional area of the tubing

Flow rate of processed water with time was studied using Dolomite Mitos Sensor Unit, comprising of Mitos Sensor Display and an attached Mitos Flow Rate Sensor (3200096). This unit was attached to the filtration unit via peristaltic pump arrangement. Figure 14 illustrates pictorial arrangement made to read flow rate of processed water with time. Tap water was used as a reference to understand the fluctuations/trend in flow of the given sample.

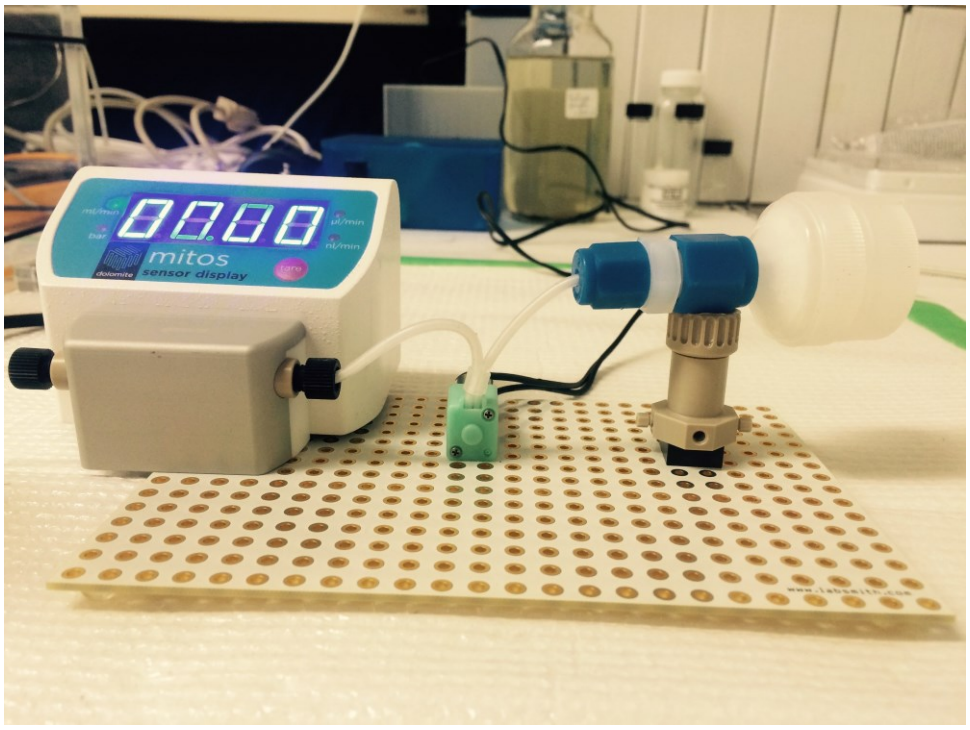

Figure 14 Pictorial arrangements made to understand the flow rate of processed water with reference to tap water

Flow rate of sample, viz., processed water with time in reference to tap water is given in Figure 15. Data has been made more readable by 0.125 Hz Low Pass fft filter for both the sample and water.

In figure 15, it was observed that a comparatively smooth plot with fewer peaks was obtained for tap water. However, plot for flow rate of the sample observed frequent peaks. This shows that flow rate of the sample was not very consistent owing to factors mentioned above. A more erratic fall and rise of flow rate occurred after 98th minute of experimental run. Backpressure was observed for both sample and water.

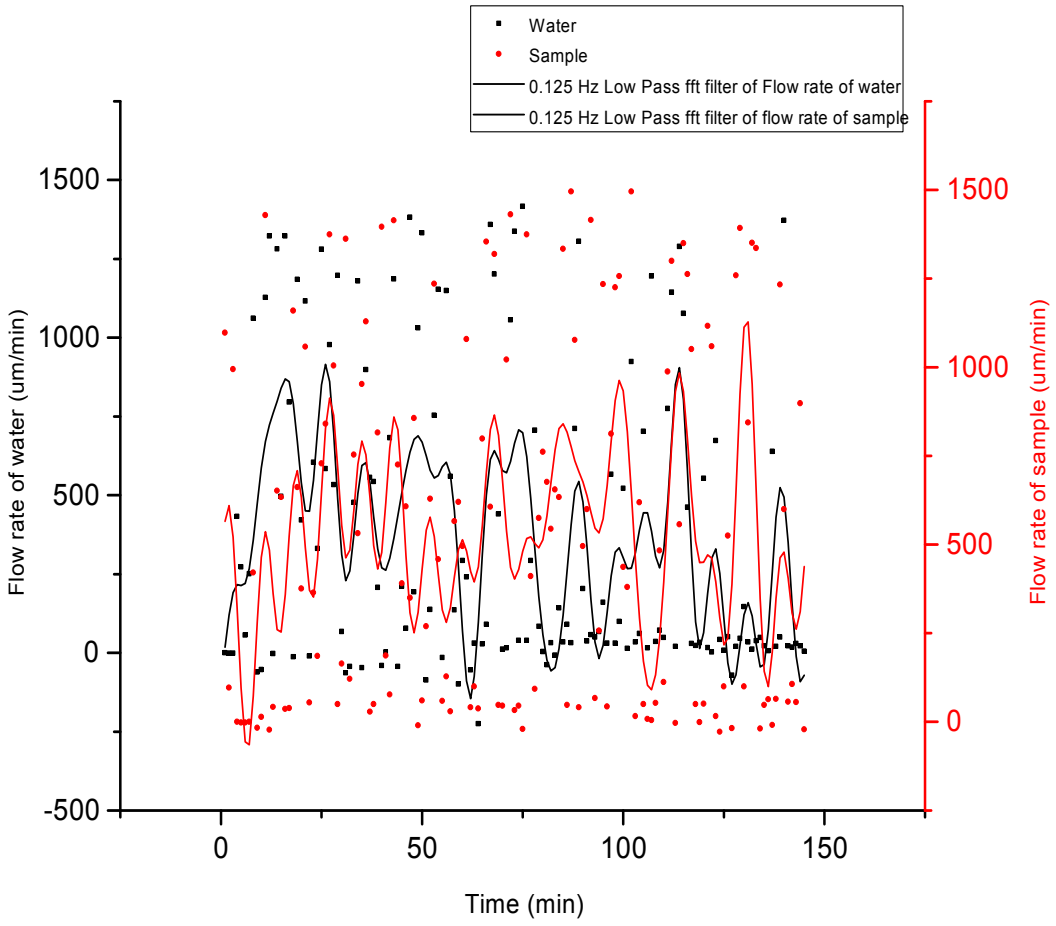

Figure 15 Flow rate of sample with time in reference to flow rate of tap water

4.7 Pump Performance

The performance of the pump played an important role in running the system. The count of droplets of sample on the copper plate enclosed in heating unit was largely affected by pump efficiency. As discussed already, cake formation occurs on the filter membrane with the passage of particulates laden sample through it. With time, this cake layer demands the pump use more power so as to maintain its best maximum output flow. In turn, this affects the pressure and flow rate of the sample. It is, thus, inevitable to understand how pump used in the system functions for the sample provided by IOSI. Tap water was used as a reference fluid to have a better understanding of pump performance.

Pressure transducer was used to measure the pressure alongside flow rate that was measured with Mitos unit. Pressure measured in psi was converted to its respective pressure head (feet) using the below conversion

$$H_P = \frac{P}{S.G. \times g.} \tag{4.5}$$

Where,

H_P is pressure head in feet

P is the pressure in psi

S.G. is the specific gravity of the sample. Specific gravity of the sample is taken to be 1.0 at 21.1°C as most of the sample is constituted of water.

The hydraulic head of a fluid, in simplified form of Bernoulli Principle, is composed of Pressure head and Elevation head. The latter component of head is the potential energy of the fluid due to its elevation. The head equation can, thus, be written as

$$H = H_P + z \tag{4.6}$$

Where,

H is the hydraulic head of the system

H_P is the pressure head that was found as mentioned above

z is the elevation given in units of length, viz., meter or feet. The elevation head can be omitted in our system, as it does not bear a large value.

Head losses, viz., minor and major losses are associated with a flowing fluid. It is important to bring into account the losses associated in the system as well. Head losses can be found using Darcy-Weisbach equation. This equation relates to head loss due to friction along the length of the pipe with the flowing fluid. It also contains a dimensionless factor, widely known as Darcy friction factor.

Darcy-Weisbach equation in terms of pressure loss is given as

$$\Delta P = f_D \frac{L}{D} \frac{\rho u^2}{2} \tag{4.7}$$

Where,

ΔP is the pressure loss

L is the length of pipe

D is the hydraulic diameter of the pipe

u is the velocity of flow measured as volumetric flow rate per cross-sectional area

g is the acceleration due to gravity

f_D is Darcy friction factor that can be found using Moody diagram. For a fully developed laminar flow, Darcy friction factor is simplified as

$$f_D = \frac{64}{Re} \tag{4.8}$$

Where, Re is Reynolds number. For fluidic system, the mean velocity of the fluid is 0.45 ml/min flowing through a length of 20 cm. We can calculate the entrance length of fluid in the tubing using formula as given

$$\frac{l}{D} = (0.06)Re \tag{4.9}$$

It was found that the entrance region was 2 cm, which was much smaller than the length of rest part of the tubing being 10 cm. Since, most part of the tubing has fully developed laminar flow, we have used aforementioned Darcy friction factor. Assuming the sample as water for the major part of it being water, its kinematic viscosity at 21.1°C would be 1.924×10^{-5} ft^2/s. For the given conditions, Reynolds number is 475 approximately resulting in Darcy friction factor to be 0.1 for the arrangement. The value of pressure loss could be neglected as it is very low, being 0.00012 Pa. Eventually, this would result in a very low head loss. Head loss can, thus, be omitted from the system.

Therefore, head of the system would largely contain pressure head of the sample flowing through the tubing of hydraulic diameter 1.5 mm. Figure 16 shows peristaltic pump performance in terms of pressure head (ft.) vs. flow rate (um/s) of both the water

and sample. A linear fit was plotted separately for water and sample data to understand pump performance in a better way.

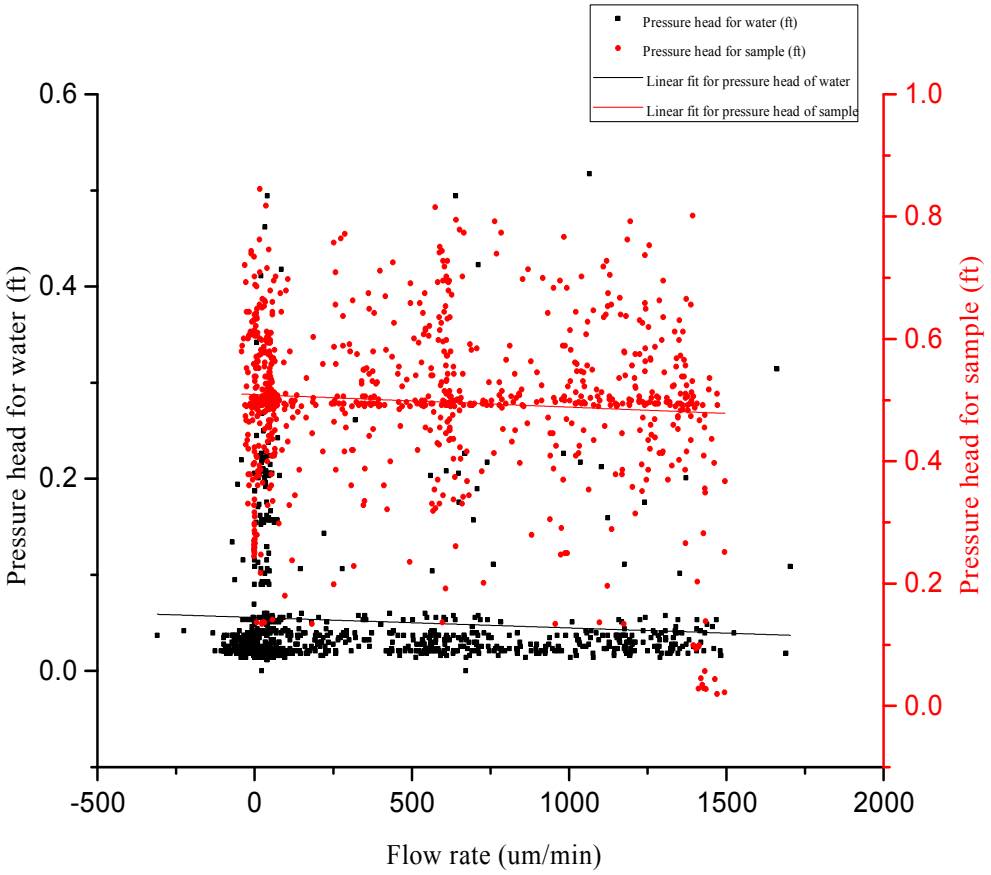

Figure 16 Pump performance for sample with reference to tap water in terms of pressure head vs. flow rate of fluid

From the graph of pump performance for water and sample, it can be observed that there is a gradual reclining plot. Pressure head decreases with the increase in flow rate of both water and sample. However, intercept for pressure head for sample was higher than that of water. This implies that more pressure was exerted on the fluid for sample flow. Traversing particulates and other particles with the sample has brought about this difference. Surprisingly, slope for both water and sample was found to be relatively the

same. The arrangement was run for 183 minutes as filter membrane was found to rupture at 182th minute, discussed in section 4.2.

4.8 Fluidic System Performance

For Naphtha detection in the sample, fluidic delivery set-up was attached to photothermal cantilever deflection spectroscopy arrangement, which was work, conducted by Prof. Thomas and group. This work is detailed elsewhere. (Bagheri, Chae et al. 2014) Figure 17 shows the complete naphtha-detecting device obtained after attaching the fluidic delivery arrangement to the photothermal cantilever deflection spectroscopy one.

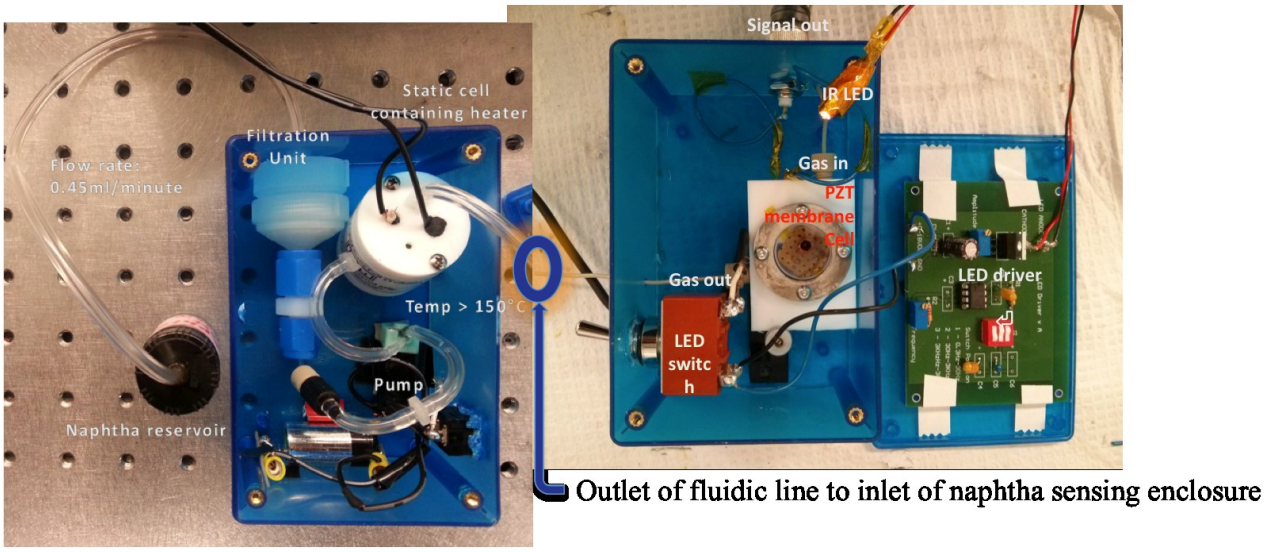

Figure 17 Real view of complete naphtha-detecting device obtained after attaching the fluidic arrangement to the photothermal cantilever deflection spectroscopy

Naphtha was detected using the aforementioned device for the sample provided by IOSI. Figure 18 shows the data of naphtha obtained for the sample. A smooth data was plotted to the otherwise noise in the original data. As an extended work to detect naphtha,

adding more naphtha to the original sample increased naphtha concentration in the sample. Naphtha was then detected by running the setup for 800 seconds. This is shown in figure 19. Figure 20 gives a plot of amplitude (mV) with the naphtha concentration found in the revised sample.

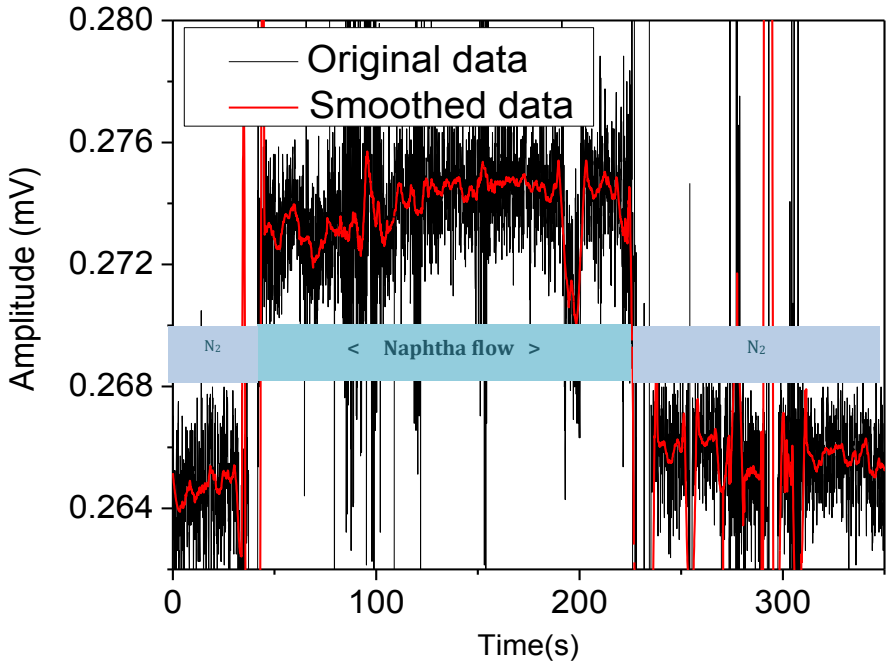

Figure 18 Naphtha detection using the complete assembly

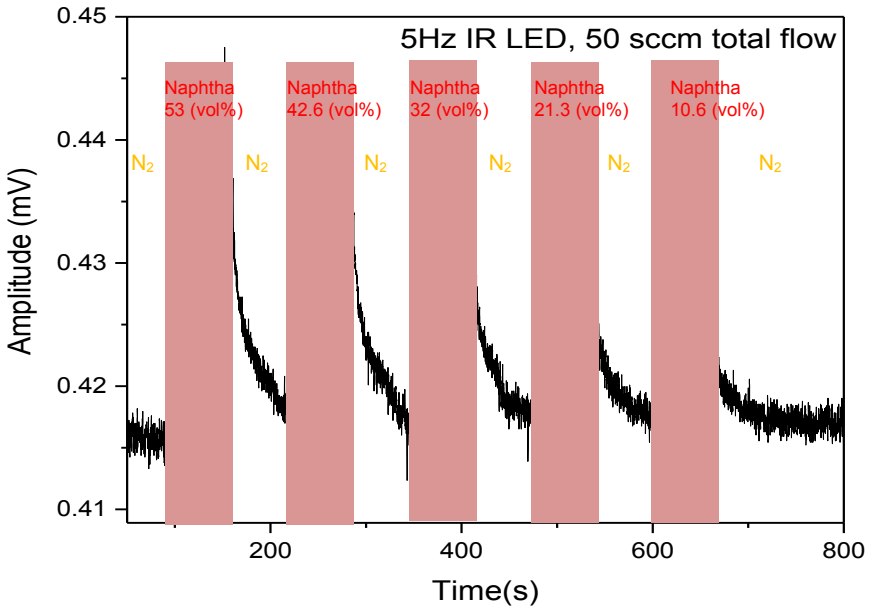

Figure 19 Naphtha detection in the sample during an experimental run of 800 seconds

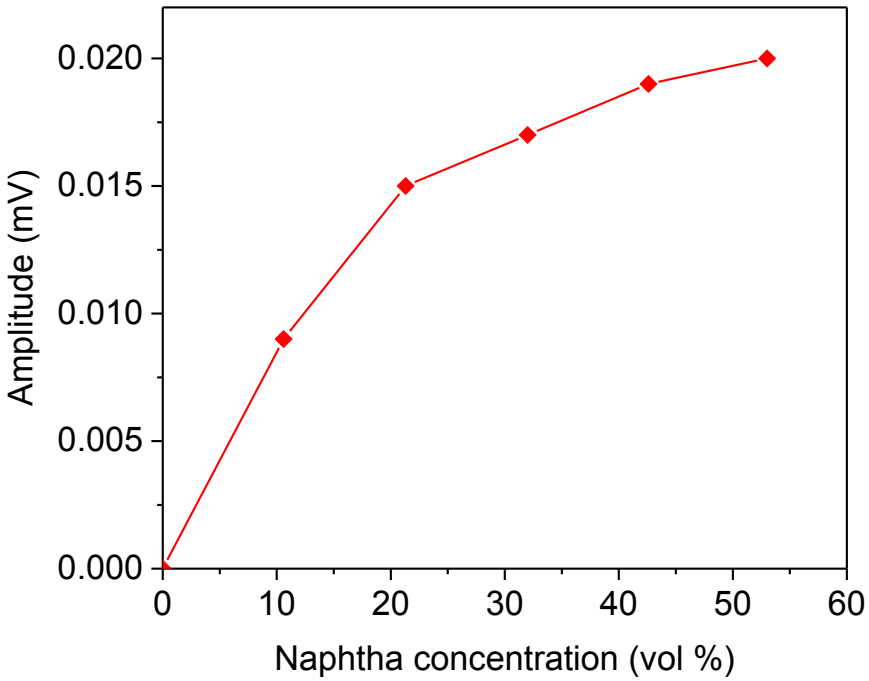

Figure 20 Plot of amplitute (mV) with Naphtha concenetration

4.9 Specification of the fluidic delivery system for naphtha detection

Specification of the fluidic delivery system for naphtha is tabulated in table 1. It highlights the basic framework of the aforementioned system. The operating ranges of temperature, pressure and flow rate have been noted from the readings obtained after running the system on the whole. This could result in deviation of the readings from those of individual component. Reasons for such deviations have been discussed in previous sections of this chapter already. This tabulation gives the main specifications of the fluidic delivery system concerned with Naphtha detection. It is to be noted that power supply in the final work has been replaced with a battery to enclose the system within the system. Replacement of the battery would be required as well.

Table 1 Specifications of fluidic delivery system for naphtha detection

Seat Material	Filtration Unit	Polypropylene
	Heating Unit	Polytetrafluoroethylene
	Tubings	Silicone
	Heating plate	Copper and Mica
	Heating element	Nichrome
Operating Temperature Range	Maximum: 225°C	Minimum: 100°C
Operating Pressure Range	Maximum: 0.35 psi	Minimum: 0.01 psi
Flow rate of working fluid	Maximum: 1200 μm	Minimum: 150 μm
Dimension	Width	10 cm
	Length	13cm
	Height	8cm
Pump length of service	Peristaltic pump	500 hours
	Diaphragm pump	640 hours
Life of Filter Membrane	Based on system continuous run	3 hours 2 minutes

Chapter 5 Proposing Model-II for fluidic delivery system

5.1 Motivation to propose a second model for fluidic delivery system

Fluid delivery set-up detailed in previous sections used heat to vaporize the fluid. In a more remote environment, eliminating power consumption by a system would be a wise decision. Keeping into consideration a more remote scenario, a second model is proposed which can be used as future work. In addition to reducing power consumption, this model is expected to provide better filtration, light in weight, waterproof and cantilever storage would be within the set-up. Power consumption would be only by the peristaltic pump used to draw fluid out of the filtration unit.

5.2 Wireframe outline of proposed Model-II

Model-II is composed of various components enlisted below. These components are connected using silicone tubing. They are elaborated in detail in the upcoming sections.

(a) Filtration unit to collect and filter the sample
(b) Peristaltic pump
(c) Polymethymethacrylate microfluidic chip
(d) Syringe pump arrangement
(e) Cantilever holding chamber

Figure 21 shows a schematic representation of the redesigned model. Sample container is not a part of the model. It would be scaled to a reservoir or any other site where naphtha needs to be detected in real scenario. The inlet of the fluidic delivery model would be the inlet tubing to the filtration unit while the outlet would be the sensor storage chamber wherein vapors of the sample would be collected. In the upcoming sections, both approaches made and those of which need to be made in building the components are discussed. The components readied may be used in conjugation with yet to be fabricated parts in accomplishing the complete build up of the model and put to site test.

Despite of the advantages that this model is expected to give, still further effort could be made to upgrade the system. This model can be pushed further for future work.

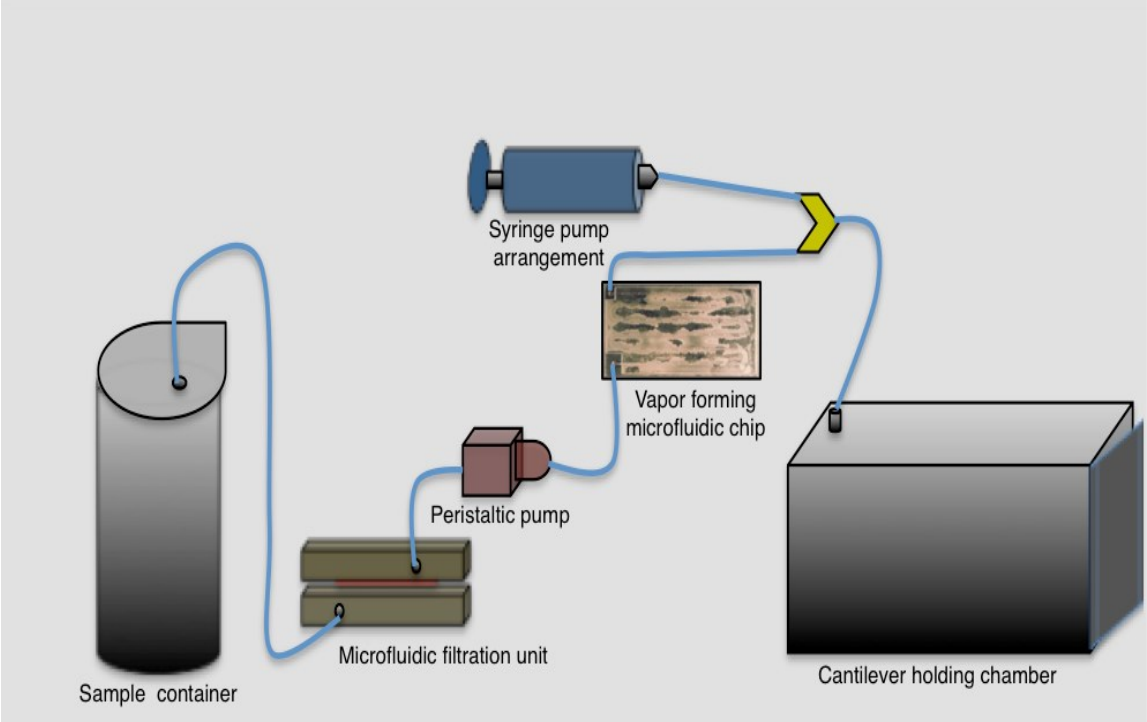

Figure 21 Schematic representation of the redesigned model

5.3 Filtration unit

The miniature pump-namely- Dolomite peristaltic pump (3200243, Dolomite Center Ltd., Charlestown, MA) producing a flow rate of 0.45ml/ min was driven by 3V power supply). The former helped pull in the sample from the storage container into Membrane chip Interface unit (3200345, Dolomite Center Ltd., Charlestown, MA) enclosing hydrophilic polytetrafluroethylene filter membrane (3200347, Dolomite Center Ltd., Charlestown, MA) with a nominal pore size of 0.2 μm and 25 mm diameter. Figure 22 shows the filtration unit comprising of the membrane chip interface (opened in the picture to give the inside view of the unit), two membrane chips, PTFE membrane filter and four chip headers FFKM Seal (supplied along with the interface). A smaller pore size

filter membrane was chosen to ensure removal of much finer particulates, if any, so as to avoid clogging of the channels ranging in micro scales.

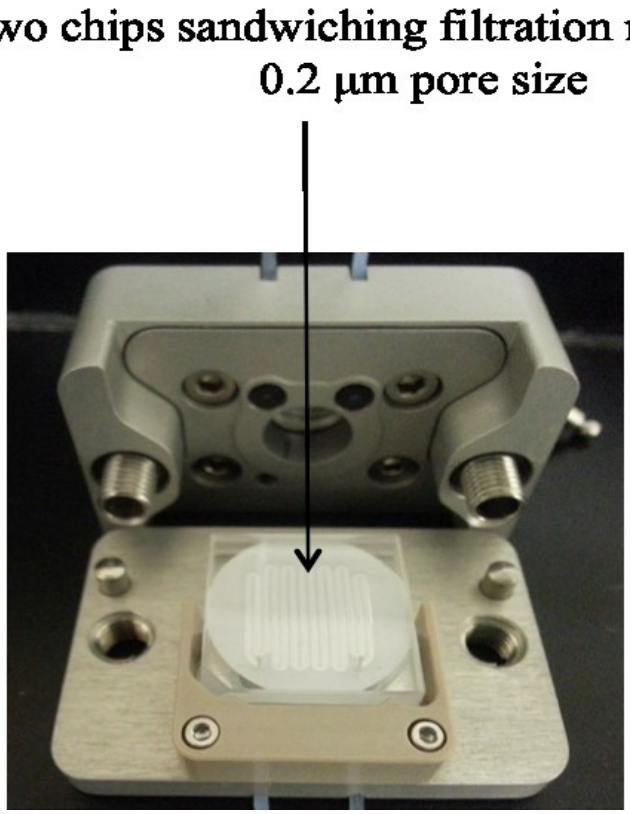

Figure 22 Filtration unit

The glass with PTFE chip in the filtration unit is fabricated using wet etching having a thickness of 4 mm and a size of 24 mm × 24 mm. The internal channel cross sectional area of the chip is 900 μm × 150 μm (W × H) having a length of 212 mm. Unlike previously used filter membrane of pore size 0.45 μm, the current membrane has finer pores of 0.2 μm. These specifications hold good for a better filtration of the sample.

5.4 Vapor forming microfluidic chip

Phase change from liquid to its vapor form is facilitated within a microfluidic chip. This chip is fabricated of Polymethymethacrylate (PMMA) material by manually etching them. Microfluidic chip consist of three etched layer, viz., base layer, sandwiched layer

and a top layer, screwed together. Rubber linings were made beside the outer etched channels to provide better gripping of the chips. Figure 23 gives a real view of the fabricated microfluidic chip.

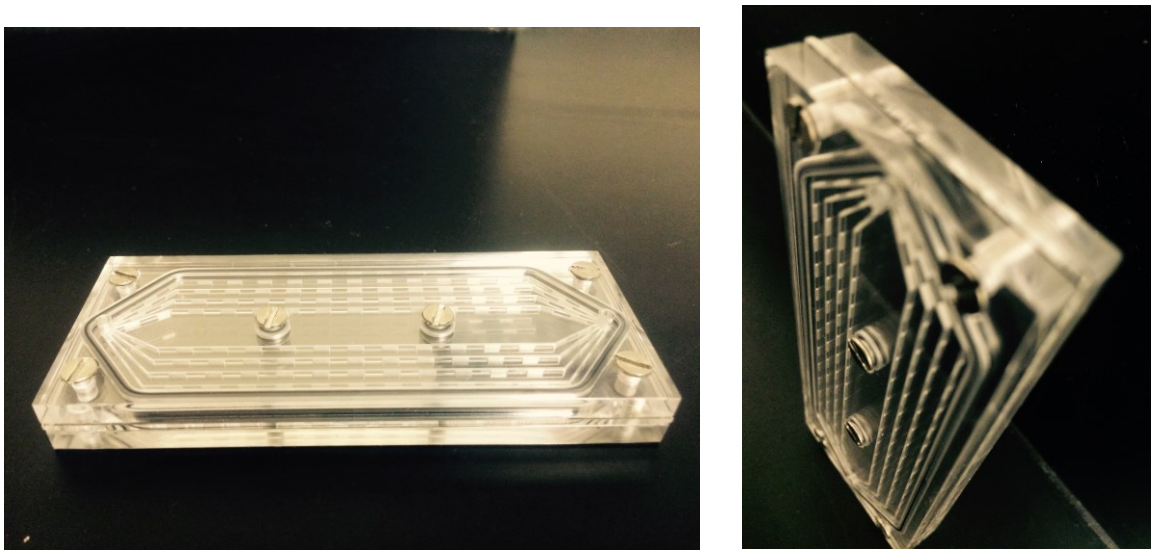

Figure 23 Real view of fabricated microfluidic chip

In the fabricated chip, a total of eight channels were etched on the base layer and top layer in a way that they ran parallel to each other in major part of the active surface area of the chip. These channels were slanted on both ends to meet a common inlet and outlet openings. There were alternate openings etched on the sandwiched layer bearing the same contour as those in the base and top layers. All the channels were 462 μm × 600 μm (depth × width) with a length of 8cm. The chip enclosure dimension is 40.3 mm × 100mm × 14 mm (width × length × height). Six screws were used to grip the layers together. O-rings grooves for O-rings sitting were made around the screw openings. Figure 24 gives a pictorial view of fabrication of the vapor forming microfluidic chip. One of the most important concerns in fabricating the chip is to ensure that the etched channels are aligned exactly one over the other. Improper alignment would reduce the cross-sectional area, leading to a reduction in the sample interface available for vapor transition. Care should also be taken while tightening of the screws as exerting more

pressure could break the chip same as improper screwing could lead to sample leakage within the microfluidic chip. Etch and screw method of fabricating microfluidic chip is cost effective, much needed in industrial applications.

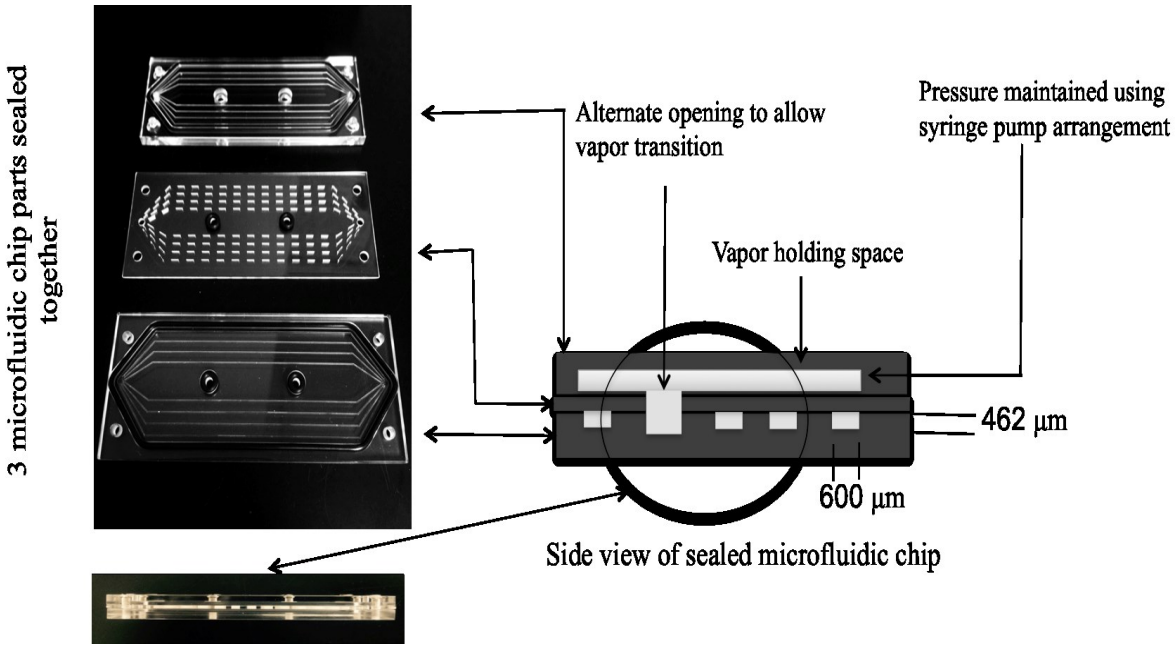

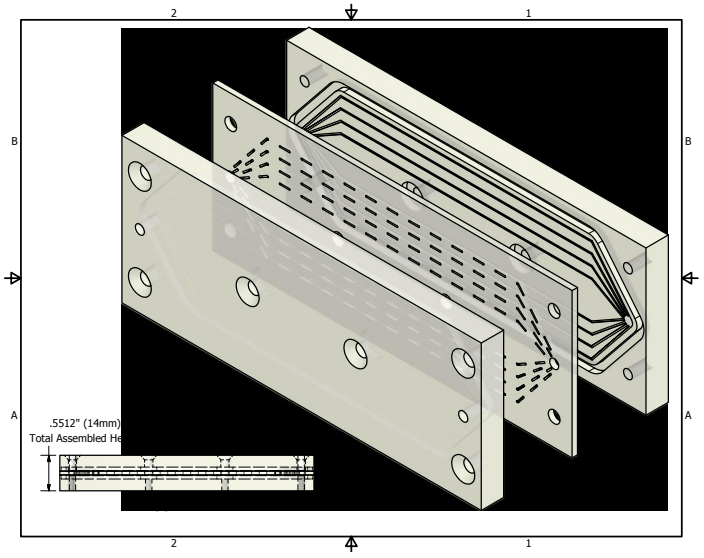

Figure 24 Fabrication of vapor forming microfluidic chip

Vapor transition from liquid state is expected to take place by reducing the pressure of the system to vapor pressure of the feed using a syringe pump arrangement, which will be discussed in the upcoming section. Alternate openings are made to allow the vapor to escape to the top layer, which later flows to the sensor storage chamber due to pressure difference created.

5.4 Sensor storage chamber

Unlike previous fluidic delivery system, a sensor storage chamber is incorporated in the current model. In addition to allow storing of sensor within, this chamber would also act as a variable tank in the syringe pump arrangement (discussed in next section) to maintain the desired pressure in the system. It has a cuboidal structure and is made of Plexi-glass. One of the faces can be opened easily for storing the sensor or draining the vapors. It is airtight with a small opening at the top to connect the tubing to the outlet of microfluidic chip. Two detachable O-rings are provided around the chamber to give the opening face an extra hold against the chamber. The current chamber has a dimension of 19 cm × 13 cm × 13 cm (length × width × height), calculated to meet the desired vapor pressure of the sample in the whole arrangement. The walls of the chamber are 1 cm thick. This leaves internal volume of the chamber to be 2057 cm^3. Figure 25 gives a real view of the sensor storage chamber. Adjoining figure shows the open face of the chamber.

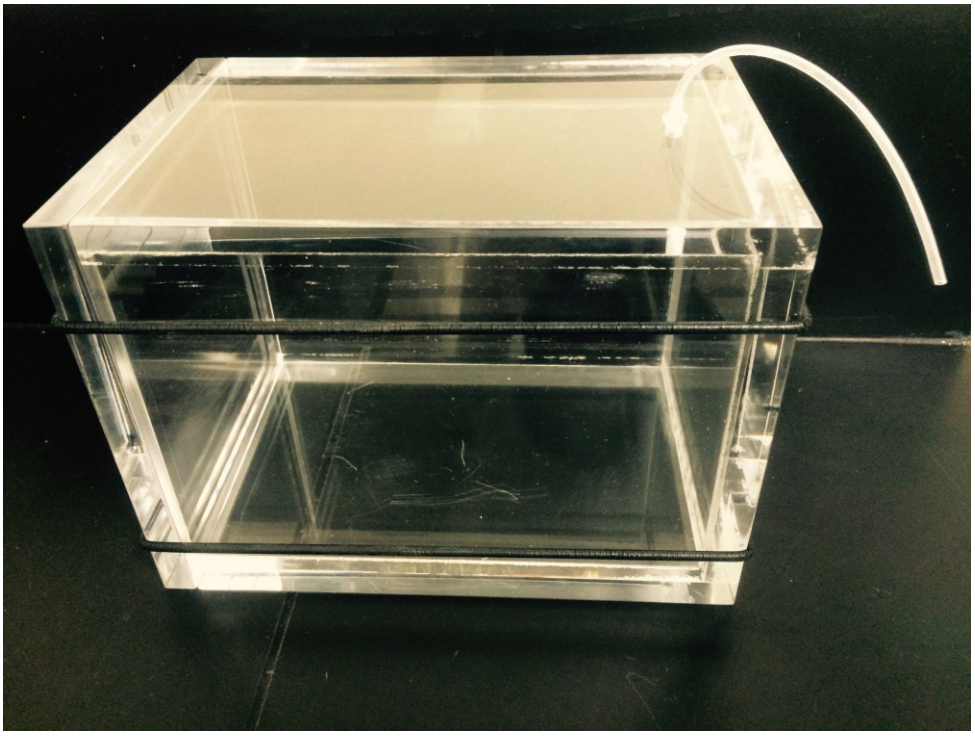

Figure 25 Real view of Sensor storage chamber

5.5 Syringe pump arrangement to maintain pressure of the system

Pumping is essential in several microfluidic applications, majorly, to draw feed in and out of the system. However, in this model, pumping would be used to maintain pressure for vapor transition in the system. The knowledge of syringe pump arrangement for maintaining pressure is gained from work by Chein et al. (Moscovici, Chien et al. 2010) Syringe pump arrangement uses a syringe pump, a chamber that acts as tank, V-connector and tubings. The chamber used is the one as discussed in the section 5.4.

In any given system, a change in volume of confined gas brings about a change in pressure. According to equation of state, PV= constant, where, P is pressure and V is the volume of the gas. This concept would be used in the system to meet the desired pressure, which is the vapor pressure of the sample. Figure 26 illustrates the syringe pump arrangement and its working principle. Variable tank in the work of Chein et al. is replaced with chamber that has an internal volume of 2057 cm^3. Change in the volume is

made by syringe pump connected to the chamber and microfluidic chip using a T-connector.

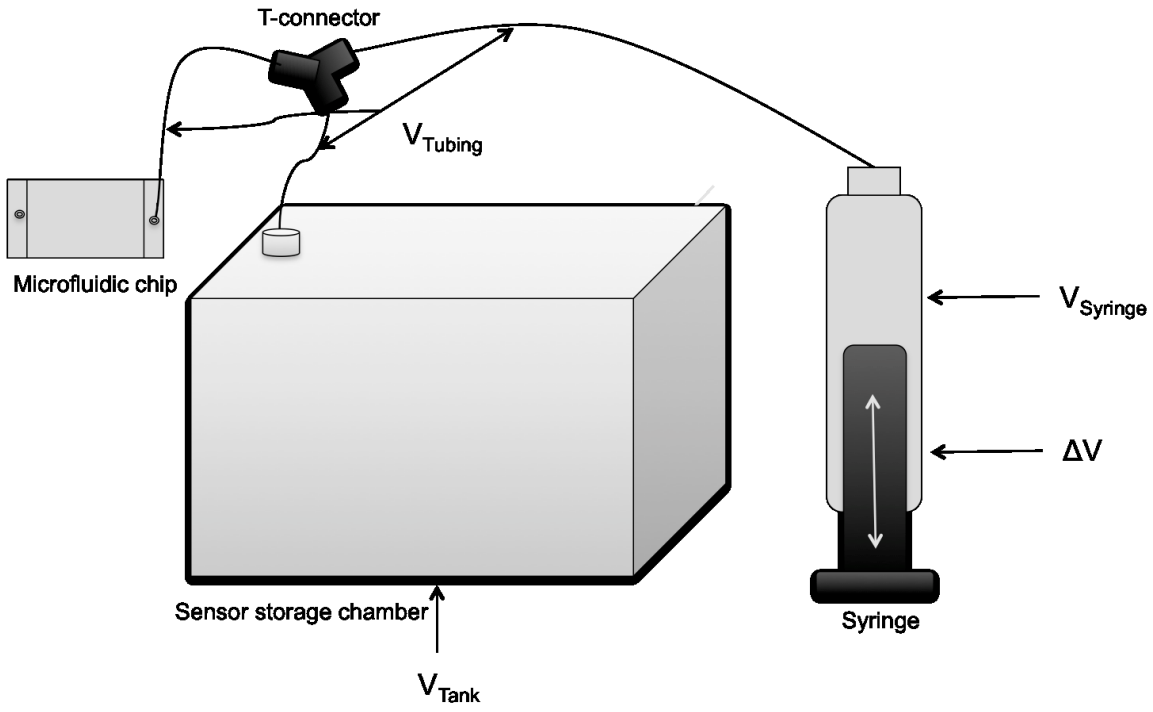

Figure 26 Syringe pump arrangement and its working principle

An increment of in the volume, ΔV, of the system is obtained by pulling the plunger in outward direction of the syringe. To calculate the pressure needed for a system, Chein formulation shall be used, as given

$$P_{system} = -P_{atm}\left(\frac{\Delta V}{V_{total}+\Delta V}\right) \quad (5.1)$$

Where,

P_{atm} is the atmospheric pressure

ΔV is the increment in volume of the confined gas

V_{total} is the initial volume of the system. V_{total} can be segmented as given

$$V_{total} = V_{tubing} + V_{tank} + V_{syringe} \quad (5.2)$$

The variables in the above equation are as those shown in figure 26. $V_{syringe}$ is the initial volume of the syringe before undergoing any change in volume, viz., ΔV.

As discussed in section 5.4, sensor storage chamber has an internal volume of 2057 cm^3. Tubings used have an internal diameter of 1.5 mm with a total length of 40cm. Internal volume of microfluidic surface active channels would be 2.7×10^{-8} cm^3. To ensure vapor formation of sample, in particular naphtha, pressure above the sample interface in the microfluidic chip should be equal to the vapor pressure of naphtha. Knovel solvent properties database gives the vapor pressure of Shell VM&P naphtha HT as 1.5 kPa. This desired pressure would be maintained by increment in volume of the system, viz., ΔV. It is of utmost importance to choose the right volume of syringe for appropriate overall internal volume where the pressure is to be maintained. Upon calculation using equations given above and keeping P_{system} to 1.5 kPa, we can find the volume of syringe needed for the syringe pump arrangement. For maintaining a pressure of 1.5 kPa in the system, syringe pump arrangement would employ a syringe with an internal volume of 812 ml. This volume can be achieved by arranging seven 100 ml syringe and one 120 ml syringe in parallel connection by letting the output tubings to a common leg of T-connector. The footprint of this syringe arrangement is expected to be same as that of the chamber and can be fixed on the larger face of the chamber to maintain overall footprint of the model. Figure 27 shows the best possible alignment of seven-syringe arrangement from side view of the system indicated in figure 26 to achieve minimum footprint. The blue syringe is the variable syringe for which the movement of plunger is expected to maintain the pressure required in the system.

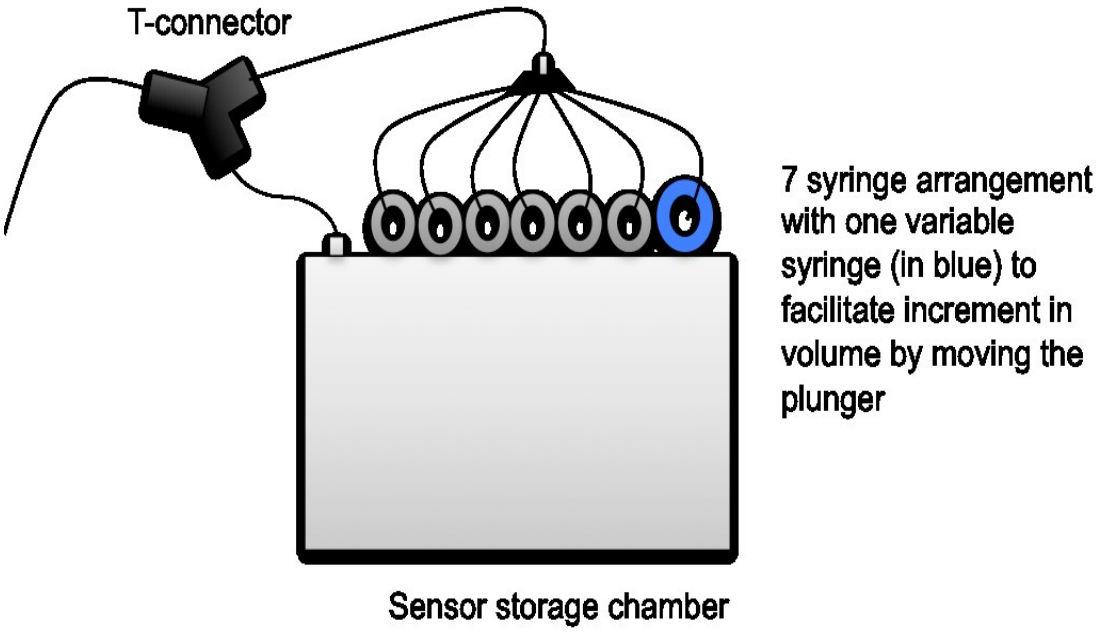

Figure 27 Expected alignment of seven-syringe arrangement to achieve minimum footprint

5.6 3D printed microfluidic chip interconnect

Moving a fluid from macro environment, viz., reservoir, to micro one, viz., microfluidic chip, is one of the major concerns. Conventional practices involve fitting tubings on the holes punched in the chip as elaborated in chapter 2. Over the years, substantial improvements have been made in designing an interconnect. Of all the available approaches in making an interconnect, 3D printed interconnect is chosen for the model to hasten work at lower cost without compromising with the benefits it offers to other approaches. The single inlet and outlet interconnects were designed using Solidworks software (Solidworks Education edition 2014-2015) and printed using a 3D printing service (Object 3D printer, Stratasys). The interconnect bears clipping mechanism to hold on to the microfluidic chip. The interconnect presented combines two types of elastomers, viz., a flexible Tango Black Plus and a rigid Vero Gray material. The design was converted to .stl to convert data in Solidworks to end user model for 3D printing. Figure 28 shows the 3D printed parts in different views and the two components that goes

into making the interconnect. These two components are combined manually without the used of any adhesive. Due to the elasticity of Tango Black Plus material, the inside O-structure can be pushed inside the hole of rigid structure with much ease. The O-structure clings against the walls of the hole to ensure there's no air passage.

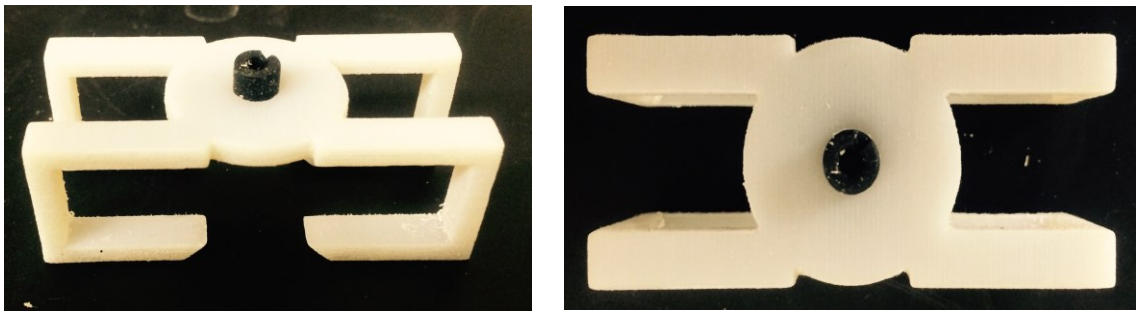

(a) **(b)**

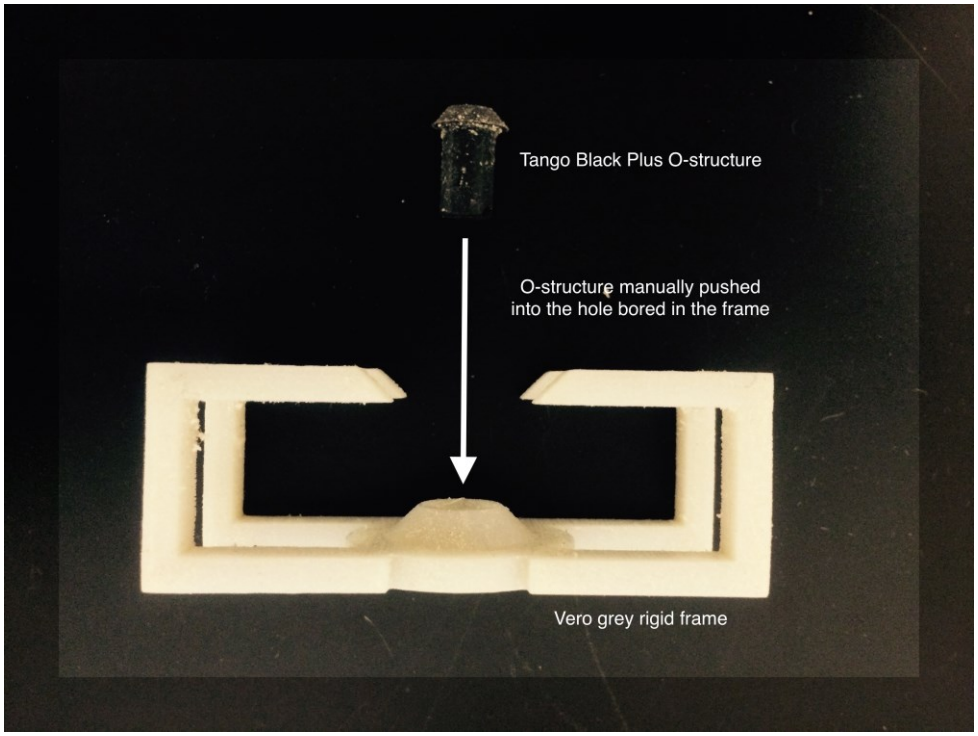

(c)

Figure 28 3D printed microfluidic interconnect (a) overall view of interconnect (b) top view (c) side view of two parts that goes into assembling of the interconnect

The presented 3D printed interconnect is incorporated at both ends of the vapor forming microfluidic chips wherein it serves as inlet and outlet interconnect. The O-structure has an inner diameter equal to the tubing outer diameter, which is also fitted using manual push-in mechanism. Figure 29 shows real views of the 3D printed interconnect, holding tubing, incorporated at one end of the vapor-forming microfluidic chip.

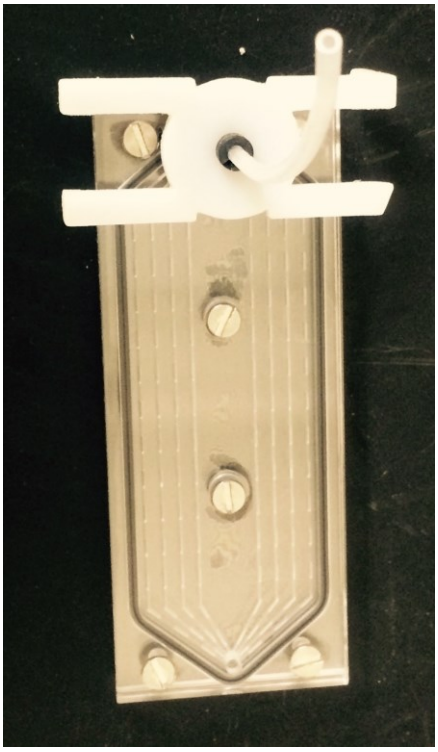

Figure 29 3D printed interconnect incorporated in one side of vapor forming microfluidic chip

In addition to being low cost and low time required for printing, 3D printed interconnect ensures that whole of the incoming fluid is transported to the microfluidic chip with much ease. This provides better performance of the system ensuring no mass transfer deviation occurs. Furthermore, it has a capability of withstanding more pressure owning to its rigid frame. The printed clamp and gasket interconnect is also easy to incorporate onto the microfluidic chip by sliding the chip against the legs of the interconnect. The only cons of the interconnect are that they are custom designed for particular chips, thereby losing its versatile application.

5.7 Pressure-Volume relationship for the system

An ideal environment is maintained in section 5.5 for vapor pressure of naphtha and hence the volume required in achieving the desired pressure. However, vapor pressure of feed changes with changing temperature. It is also dependent on the feed constituents, viz., pure feed or a mixture of feed. It is of utmost importance to understand the varying vapor pressure according to the environmental conditions and the volume that needs to be maintained in the system accordingly. A simple pressure-volume relationship for the system in a given environment is defined in this section.

Clausius-Clapeyron equation is widely used to estimate vapor pressure of a liquid (or solid). Assuming the vapors formed by the fluidic delivery system behave as ideal gases, equation is given below

$$\ln \frac{P}{P^{\circ}} = \frac{\Delta H}{R}\left(\frac{1}{T^{\circ}} - \frac{1}{T}\right) \tag{5.3}$$

Where,

P is the vapor pressure in the source environment

P° is the vapor pressure of feed at a known temperature T°

ΔH is the enthalpy of vaporization for the liquid (feed)

T is the temperature of the environment

R is the ideal gas constant. For the system, we are interested in finding P and the volume to maintain this pressure for feed to vaporize.

An increment in the volume of the system, ΔV, in a given environment having temperature T can be calculated by using Clausius-Clapeyron equation with Syringe pump arrangement equation discussed in section 5.5. This increment can be obtained by pulling the plunger in outward direction of the syringe or vice-versa for a decrement in the volume. Combining the aforementioned equations leads to below given formulation:

$$\Delta V = \frac{P^{\circ} V_{total}}{P_{atm}\left(e^{\frac{\Delta H}{R}\left(\frac{1}{T^{\circ}} - \frac{1}{T}\right)}\right)^{-1} + P^{\circ}} \tag{5.4}$$

Where,

P_{atm} is the atmospheric pressure

ΔV is the increment in volume of the confined gas

V_{total} is the initial volume of the system. V_{total} can be segmented as given

$$V_{total} = V_{tubing} + V_{tank} + V_{syringe} \tag{5.5}$$

The variables in the above equation are as those shown in figure 26. $V_{syringe}$ is the initial volume of the syringe before undergoing any change in volume, viz., ΔV. Derived formulation can be used to find by how much amount the plunger needs to be displaced to maintain pressure desirable in the source environment.

The aforementioned several components can be connected using silicone tubing to devise the proposed model in a single waterproof box. This device is expected to use even by immersing the whole model inside reservoir, tailings or any other site where naphtha needs to be detected. Furthermore, the proposed model can be used for any sensor. Vapor pressure of the feed can be adjusted by rearranging the syringes in syringe pump arrangement using equations mentioned in section 5.5. This offers a more versatile platform for detecting chemicals, other naphtha as well. Unlike fluidic delivery system using heat, the proposed model cannot be run in continuous mode. However, the presented model is expected to work even in most remote environments.

5.7 Working of Model-II

Expected working of the second model in pictorial arrangement is shown in Figure 30 for a better understanding of the working fluid and its vapor collection in collecting chamber.

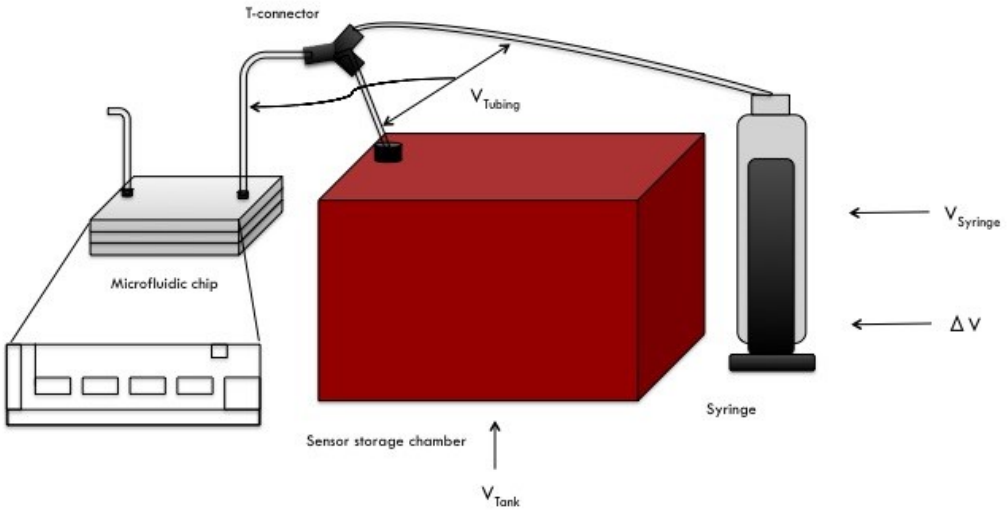
T-connector
V_{Tubing}
Microfluidic chip
$V_{Syringe}$
ΔV
Syringe
Sensor storage chamber
V_{Tank}

(a)

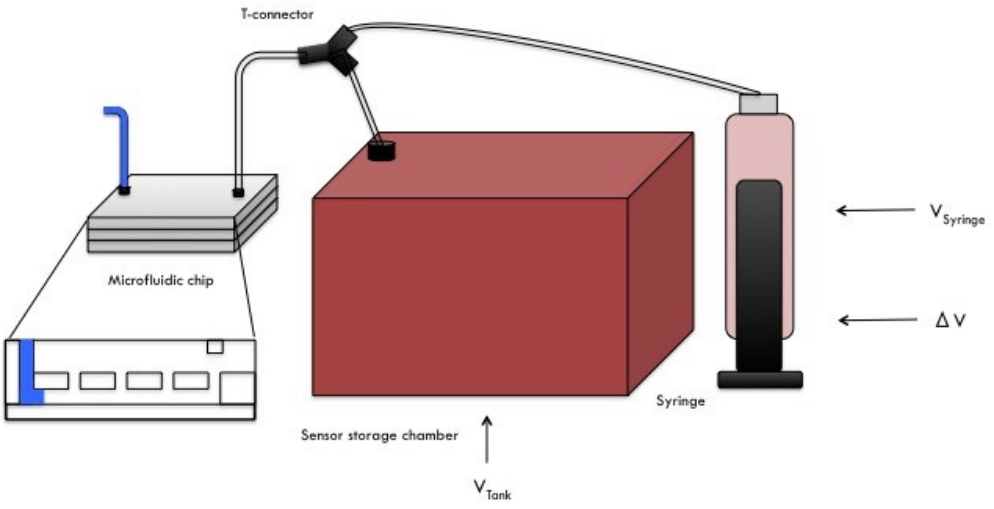
T-connector
Microfluidic chip
$V_{Syringe}$
ΔV
Syringe
Sensor storage chamber
V_{Tank}

(b)

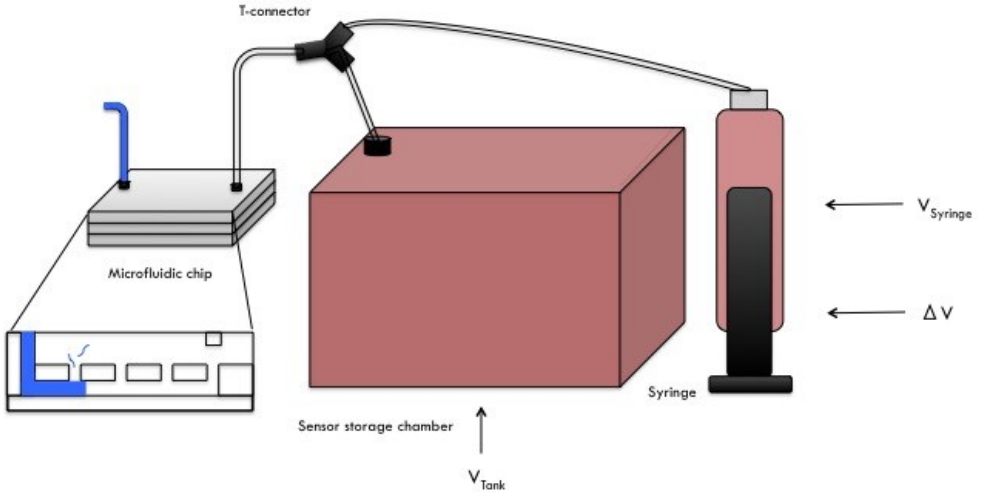
T-connector
Microfluidic chip
Sensor storage chamber
Syringe
$V_{Syringe}$
ΔV
V_{Tank}

(c)

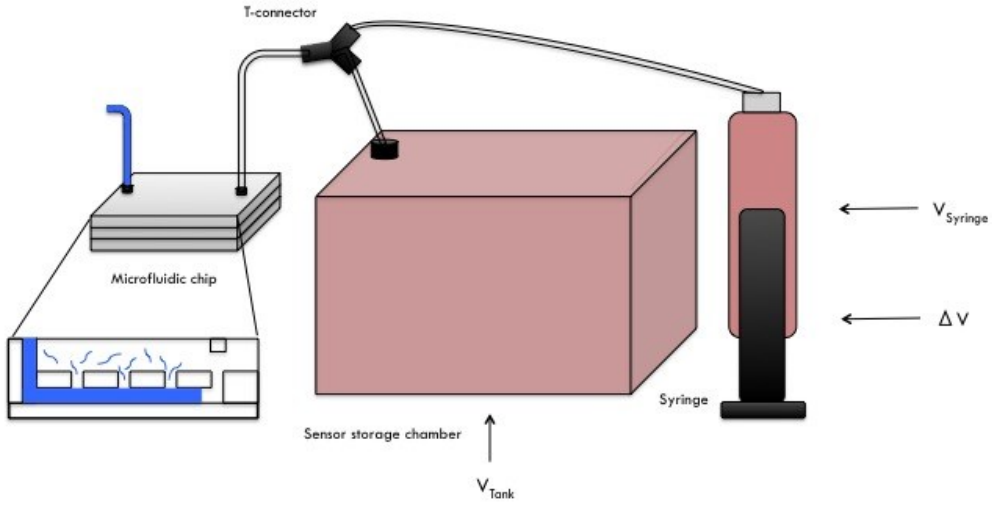
T-connector
Microfluidic chip
Sensor storage chamber
Syringe
$V_{Syringe}$
ΔV
V_{Tank}

(d)

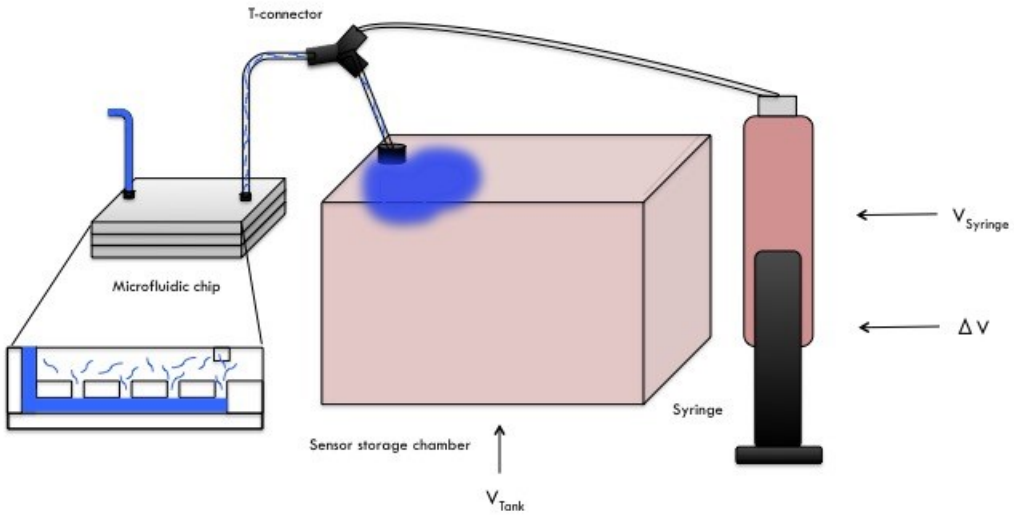

(e)

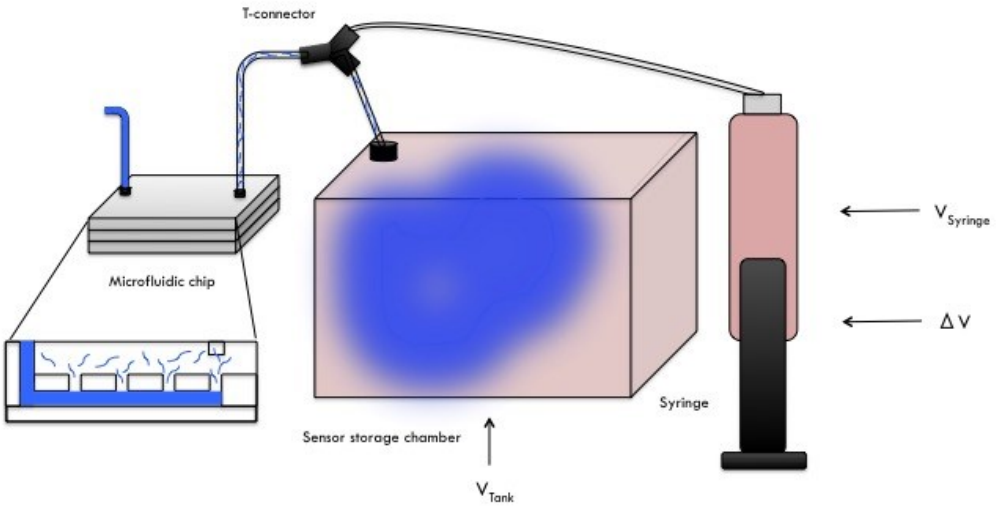

(f)

Figure 30 Expected working of Model-II (a) Static position (b) Inflow of working fluid with movement of syringe-plunger (c) First vapor formation (d) Vapor collection at the upper space of the microfluidic chip (e) Vapor inflow to the collecting chamber (f) Vapor collection

Chapter 6 Conclusions and Suggestions for Future work

6.1 Conclusions

In this study, a fluidic delivery system was designed to transport sample provided by Institute for Oil Sands Innovation, University of Alberta to the sensor it its vapor phase for naphtha detection. This system used heat to vaporize the sample falling on the heat plate in droplets. Analysis was conducted to understand the sample, viz. processed water, and working of the system. From the experimental findings, below given conclusions can be drawn:

- A fully assembled delivery system could comfortably fit in a box of dimension 10 cm*13cm*8cm (width*length*height).
- In analysis of filtration unit output as a function of mass filtrate per unit time, the membrane filter was found fully clogged after 3 hours 2 minutes. It took 12 minutes for the inlet tubing to discharge first drop of processed water to the measuring plate. It is advisable to change filter membrane in the filter holder after this time.
- pH of unfiltered and filtered processed water was found to be 8.36 and 8.92 respectively. This shows processed water sample to be more of alkaline in nature.
- Maximum volume density was shown for particles with size 12.7µm. However, minimum volume density, viz. 0.01%, was found for particle size of 186 µm. As for particle size in a filtered sample, the lower limit of the measuring equipment, viz., Mastersizer 2000, prevented measuring size of particles, if any, that persisted even after filtration.
- Flow rate of the sample observed frequent peaks with reference to tap water. This shows that flow rate of the sample was not very consistent owing to factors like filter cake formation, its configuration and thickness, size of particulates entering the feed tubing, efficiency of the pump driving the fluid in and out of the unit,

temporary accumulation of aggregates into the tubing rendering smaller cross sectional for fluid to flow, among others.

- Peristaltic pump performance showed that pressure head decreased with the increase in flow rate of both water and sample having a higher intercept for sample flow.
- Fluidic system performance was conducted for the given sample by detecting naphtha after joining the outlet of the fluidic system to the sensor system devised by Prof. Thundat and group.

Furthermore, model-II was proposed to meet a few shortcomings of the current fluidic system. Description of the work done until date in designing the proposed model and expected results has been made. The proposed model is expected to meet below enlisted advantages over fluidic system using heat:

- Reducing power consumption
- Provide better filtration
- Waterproof and,
- Sensor arrangement storage would be within the set-up.

6.2 Suggestions for Future work

It is recommended that further work could be conducted in refining the fluidic delivery system for remote environment. An approach to build an automated arrangement to maintain the pressure within the system can be made. This would lead the functioning of model in continuous mode. Joining of the three-microfluidic layers to form the vapor forming microfluidic chip can be done using wax bonding wherein the layers are attached using wax under specific conditions. This could attach and seal the layers in a better way than screwing mechanism. Analysis on the performance of the proposed system should be made to understand its working over the current fluidic delivery system.

REFERENCES"<Analysis of Phosphate in Wastewater Using an Autonomous Microfluidics-Based Analyser .pdf>."

"<ERCB report 2012.pdf>."

"<Physics in oil sands.pdf>."

(1982). Constant Pressure Blocking Filtration Laws - Application To Power-law Non-newtonian Fluids, Rugby Inst Chemical Engineers, 1982.

(2004). "A review of micropumps." Journal of Micromechanics and Microengineering **14**(6): R35.

(2010). In situ monitoring of environmental water quality using an autonomous microfluidic sensor, Institute of Electrical and Electronics Engineers, 2010-02-23.

Aslam, M., et al. (2015). "Analysis of membrane fouling with porous membrane filters by microbial suspensions for autotrophic nitrogen transformations." Separation and Purification Technology **146**: 284-293.

Bagheri, M., et al. (2014). "Selective detection of physisorbed hydrocarbons using photothermal cantilever deflection spectroscopy." Sensors & Actuators: B. Chemical **191**: 765-769.

Beaton, A. D., et al. (2011). "An automated microfluidic colourimetric sensor applied in situ to determine nitrite concentration." Sensors & Actuators B: Chemical **156**(2): 1009-1014.

Becker, H. and L. E. Locascio (2002). "Polymer microfluidic devices." TALANTA **56**(2): 267-287.

Berg, J. M., et al. (2003). "A two-stage discrete peristaltic micropump." Sensors & Actuators A: Physical **104**(1): 6.

Blair, S. M. (1951). The development of the Alberta bituminous sands. [Edmonton, A. Shnitka, Kings Printer.

Bowden, M., et al. (2002). "A prototype industrial sensing system for phosphorus based on micro system technology." The Analyst **127**(1): 1-4.

Bowden, M., et al. (2002). "Analysis of river water samples utilising a prototype industrial sensing system for phosphorus based on micro-system technology." Journal Of Environmental Monitoring: JEM **4**(5): 767-771.

Camp, F. W. (1976). The tar sands of Alberta, Canada. United States, Cameron Eng. : Denver, Colo., United States.

Carpenter, S. R., et al. (1998). Nonpoint Pollution of Surface Waters with Phosphorus and Nitrogen, Ecological Society of America**:** 559.

Clark, K. A., et al. (1927). The bituminous sands of Alberta. Edmonton, W.D. McLean, acting king's printer.

Cleary, J., et al. (2010). "In situ monitoring of environmental water quality using an autonomous microfluidic sensor." 2010 IEEE Sensors Applications Symposium (SAS): 36.

Cleary, J., et al. (2010). "Analysis of phosphate in wastewater using an autonomous microfluidics-based analyser." International Journal of Environmental Science and Engineering(3): 145.

Cymbalisty, L. M. O., et al. (1989). TREATMENT OF PRIMARY TAILINGS AND MIDDLINGS FROM THE HOT WATER EXTRACTION PROCESS FOR RECOVERING BITUMEN FROM TAR SAND. L. M. O. Cymbalisty, G. J. Cymerman, L. T. D. Alberta Energy Co et al. Canada, 478673.

Czugala, M., et al. (2013). "Portable integrated microfluidic analytical platform for the monitoring and detection of nitrite." Talanta **116**: 997-1004.

Davoust, L. and J. Theisen (2013). "Evaporation rate of drop arrays within a digital microfluidic system." Sensors and Actuators B: Chemical **189**: 157-164.

Diamond, D., et al. (2008). "Integration of analytical measurements and wireless communications -- Current issues and future strategies." Talanta(3): 606.

Díaz-González, M. and A. Baldi (2012). "Fabrication of Biofunctionalized Microfluidic Structures by Low-Temperature Wax Bonding." Analytical Chemistry **84**(18): 7838-7844.

Ei, et al. (2011). "In-situ and remote monitoring of environmental water quality."

Golobic, I., et al. (2009). "Experimental determination of transient wall temperature distributions close to growing vapor bubbles." Heat and Mass Transfer(7): 857.

Gong, X., et al. (2010). "Wax-bonding 3D microfluidic chips." Lab on a Chip - Miniaturisation for Chemistry and Biology **10**(19): 2622.

Gonzalez, C., et al. (1998). "Fluidic interconnects for modular assembly of chemical microsystems." SENSORS AND ACTUATORS B-CHEMICAL **49**(1-2): 40-45.

Gray, B. L., et al. (2014). "Capillary-driven microfluidic chips with evaporation-induced flow control and dielectrophoretic microbead trapping." **8976**: 89760Y.

Gray, M., et al. (2009). "Physics in the oil sands of Alberta." Physics Today **62**(3): 31-35.

Hall, E. S., et al. (1988). "SORPTION-SCAVENGING METHODS FOR RECOVERY OF RESIDUAL OIL FROM OIL SANDS TAILINGS STREAMS." AOSTRA Journal of Research **4**(1): 7-18.

Homayuni, F., et al. (2012). "AN EXPERIMENTAL INVESTIGATION OF VISCOSITY REDUCTION FOR PIPELINE TRANSPORTATION OF HEAVY AND EXTRA-HEAVY CRUDE OILS." PETROLEUM SCIENCE AND TECHNOLOGY **30**(18): 1946-1952.

Hudson, J. O. and W. H. Seitzer (1971). TREATING THE PROCESS WATERS FROM THE HOT WATER PROCESS FOR EXTRACTING TAR SANDS. J. O. Hudson and W. H. Seitzer. Canada.

Jeong, O. C. and S. Konishi (2008). "Fabrication of a peristaltic micro pump with novel cascaded actuators." JOURNAL OF MICROMECHANICS AND MICROENGINEERING **18**(2): 025022.

Jordan, P., et al. (2005). "High-resolution phosphorus transfers at the catchment scale: the hidden importance of non-storm transfers." Hydrology and earth system sciences.

Kabov, O. A. (2010). "Interfacial Thermal Fluid Phenomena in Thin Liquid Films." International Journal of Emerging Multidisciplinary Fluid Sciences **2**(2/3): 87-121.

Kang, S., et al. (2015). "Optimization of cross flow filtration system for Dunaliella tertiolecta and Tetraselmis sp. microalgae harvest." Korean Journal of Chemical Engineering(7): 1377.

Kobayashi, T. and S. Konishi (2012). "Microfluidic chip with serially connected filters for improvement of collection efficiency in blood plasma separation." SENSORS AND ACTUATORS B-CHEMICAL **161**(1): 1176-1183.

Lai, H. and A. Folch (2011). "Design and dynamic characterization of "single-stroke" peristaltic PDMS micropumps." Lab On A Chip **11**(2): 336-342.

Legiret, F.-E., et al. (2013). "A high performance microfluidic analyser for phosphate measurements in marine waters using the vanadomolybdate method." Talanta **116**: 382-387.

Liu, Y.-J. and D. D. Sun (2012). "Membrane fouling mechanism in dead-end microfiltration of denitrifying granular sludge mixed liquors developed in SBRs at different calcium concentrations." Journal of Membrane Science **396**: 74-82.

Lomas, M. W. and F. Lipschultz (2006). Forming the Primary Nitrite Maximum: Nitrifiers or Phytoplankton?, The American Society of Limnology and Oceanography**:** 2453.

Lynn, N. S. and D. S. Dandy (2009). "Passive microfluidic pumping using coupled capillary/evaporation effects." Lab Chip **9**(23): 3422-3429.

Ma, H.-K., et al. (2009). "Development of an OAPCP-micropump liquid cooling system in a laptop." International Communications in Heat and Mass Transfer **36**: 225-232.

Manuel, J. (2014). "Nutrient pollution: a persistent threat to waterways: point-source releases of nitrogen and phosphorus have declined dramatically since the 1970s, but nonpoint-source pollution continues to pose a significant threat to water quality." Environmental Health Perspectives(11).

Masliyah, J. H., et al. (2011). Handbook on theory and practice of bitumen recovery from Athabasca Oil Sands. Cochrane, Alta., Kingsley Knowledge Pub.

Masliyah, J. H. c., et al. (2006). Oilsands 2006. [Edmonton, Alta.], University of Alberta, Dept. of Chemical & Materials Engineering**:** 1 computer optical disc.

McGraw, C. M., et al. (2007). "Autonomous microfluidic system for phosphate detection." Talanta **71**(3): 1180-1185.

Merin, U. and G. Daufin (1990). "Crossflow microfiltration in the dairy industry: state-of-the-art." Lait (France).

Moscovici, M., et al. (2010). "Electrical power free, low dead volume, pressure-driven pumping for microfluidic applications." Biomicrofluidics **4**(4): 046501.

Najafi, A. S., et al. (2007). "A novel method of measuring electrophoretic mobility of gas bubbles." JOURNAL OF COLLOID AND INTERFACE SCIENCE **308**(2): 344-350.

Nguyen, N.-T. and X. Huang (2001). "Miniature valveless pumps based on printed circuit board technique." Sensors & Actuators: A. Physical **88**: 104-111.

Nguyen, N.-T. and S. T. Wereley (2002). Fundamentals and Applications of Microfluidics. Boston, MA, Artech House, Inc.

Paydar, O. H., et al. (2014). "Characterization of 3D-printed microfluidic chip interconnects with integrated O-rings." Sensors and Actuators A: Physical **205**: 199-203.

Picknett, R. G. and R. Bexon (1977). "The evaporation of sessile or pendant drops in still air." Journal of Colloid And Interface Science **61**: 336-350.

Quagraine, E. K., et al. (2005). "In Situ Bioremediation of Naphthenic Acids Contaminated Tailing Pond Waters in the Athabasca Oil Sands Region----Demonstrated Field Studies and Plausible Options: A Review." Journal of Environmental Science & Health, Part A: Toxic/Hazardous Substances & Environmental Engineering **40**(3): 685-722.

Ramirez-Garcia, S., et al. (2008). "Towards the development of a fully integrated polymeric microfluidic platform for environmental analysis." Talanta(2): 463.

Sengupta, S., et al. (1997). "RECOVERY, CHARACTERIZATION AND CONCEPTUAL MODELLING OF NON-BITUMINOUS ORGANIC MATERIALS FROM OIL SANDS." Canadian Journal of Chemical Engineering, The **75**(2): 379-390.

Siddique, T., et al. (2006). "BIODEGRADATION OF SHORT-CHAIN N-ALKANES IN OIL SANDS TAILINGS UNDER METHANOGENIC CONDITIONS." ENVIRONMENTAL SCIENCE & TECHNOLOGY **40**(17): 5459-5464.

Siddique, T., et al. (2007). "METABOLISM OF BTEX AND NAPHTHA COMPOUNDS TO METHANE IN OIL SANDS TAILINGS." ENVIRONMENTAL SCIENCE & TECHNOLOGY **41**(7): 2350-2356.

Surtaev, A. and A. Pavlenko (2014). "Observation of boiling heat transfer and crisis phenomena in falling water film at transient heating." INTERNATIONAL JOURNAL OF HEAT AND MASS TRANSFER **74**: 342-352.

Thokchom, A. K., et al. (2014). "Analysis of fluid flow and particle transport in evaporating droplets exposed to infrared heating." International Journal of Heat and Mass Transfer **68**: 67-77.

Wang, F. L. and V. V. Tarabara (2008). "Pore blocking mechanisms during early stages of membrane fouling by colloids." JOURNAL OF COLLOID AND INTERFACE SCIENCE **328**(2): 464-469.

Woias, P. (2005). "Micropumps—past, progress and future prospects." Sensors & Actuators: B. Chemical **105**: 28-38.

Yaroshchuk, A. E. (2008). "Negative rejection of ions in pressure-driven membrane processes." Advances in Colloid and Interface Science **139**: 150-173.

Zazoua, A., et al. (2009). "A new HRP/catalase biosensor based on microconductometric transduction for nitrite determination." Materials Science & Engineering C **29**: 1919-1922.

Zhang, Y. L., et al. (2014). "Characteristics of dynamic membrane filtration: structure, operation mechanisms, and cost analysis." CHINESE SCIENCE BULLETIN **59**(3): 247-260.

Zimmermann, M., et al. (2005). "Continuous flow in open microfluidics using controlled evaporation." Lab Chip **5**(12): 1355-1359.

Ziolkowski, B., et al. (2012). "Integrating stimulus responsive materials and microfluidics: The key to next-generation chemical sensors." Journal of Intelligent Material Systems and Structures **24**(18): 2221-2238.